




Winter 10-28-2019

Dextran-coated Iron Oxide Nanoparticles as Biomimetic Catalysts for Biofilm Disruption and Caries Prevention

Yuan Liu
liuyuan1@upenn.edu

Follow this and additional works at: https://repository.upenn.edu/dental_theses

 Part of the [Nanotechnology Commons](#), [Oral Biology and Oral Pathology Commons](#), and the [Pediatric Dentistry and Pedodontics Commons](#)

Recommended Citation

Liu, Yuan, "Dextran-coated Iron Oxide Nanoparticles as Biomimetic Catalysts for Biofilm Disruption and Caries Prevention" (2019). *Dental Theses*. 47.
https://repository.upenn.edu/dental_theses/47

This paper is posted at ScholarlyCommons. https://repository.upenn.edu/dental_theses/47
For more information, please contact repository@pobox.upenn.edu.

Dextran-coated Iron Oxide Nanoparticles as Biomimetic Catalysts for Biofilm Disruption and Caries Prevention

Abstract

Biofilms are surface-attached bacterial communities embedded within an extracellular matrix that create localized and protected microenvironments. Acidogenic oral biofilms can demineralize the enamel-apatite on teeth, causing dental caries (tooth decay). Current antimicrobials have low efficacy and do not target the protective matrix and acidic pH within the biofilm. Recently, catalytic nanoparticles were shown to disrupt biofilms but lacked a stabilizing coating required for clinical applications. Here, we report dextran-coated iron oxide nanoparticles termed nanozymes (Dex-NZM) that display strong catalytic (peroxidase-like) activity at acidic pH values, target biofilms with high specificity, and prevent severe caries without impacting surrounding oral tissues *in vivo*. Nanoparticle formulations were synthesized with dextran coatings (molecular weights from 1.5 to 40 kDa were used), and their catalytic performance and bioactivity were assessed. We found that 10 kDa dextran coating provided maximal catalytic activity, biofilm uptake, and antibiofilm properties. Surprisingly, dextran coating also enhanced selectivity toward biofilms while avoiding binding to gingival cells. Mechanistic studies indicated that iron oxide cores were the source of catalytic activity, whereas dextran on the nanoparticle surface provided stability without blocking catalysis. Dextran-coating facilitated NZM incorporation into exopolysaccharides (EPS) structure and binding within biofilms, which activated hydrogen peroxide (H₂O₂) for localized bacterial killing and EPS-matrix breakdown. In combination with low concentration of H₂O₂, Dex-NZM inhibited biofilm accumulation on natural teeth in a human-derived *ex vivo* biofilm model, and prevented acid damage of the mineralized tissue. Furthermore, Dex-NZM/H₂O₂ treatment significantly reduced the onset and severity of caries lesions (vs control or either Dex-NZM or H₂O₂ alone) without adverse effects on gingival tissues or oral microbiota diversity *in vivo*. Therefore, dextran-coated nanozymes have potential as an alternative treatment of a prevalent and costly biofilm-induced oral disease.

Degree Type

Thesis

Degree Name

DScD (Doctor of Science in Dentistry)

Primary Advisor

Dr. Hyun (Michel) Koo, DDS, PhD

Keywords

Dextran-coated nanoenzyme, Iron oxide, Nanoparticle, Biofilm, Dental caries, Antibacterial, Extracellular matrix

Subject Categories

Dentistry | Nanotechnology | Oral Biology and Oral Pathology | Pediatric Dentistry and Pedodontics

**Dextran-Coated Iron Oxide Nanoparticles as Biomimetic Catalysts
for Biofilm Disruption and Caries Prevention**

Yuan Liu, DDS, PhD

A Dissertation

Presented to the Faculties of the University of Pennsylvania in Partial Fulfillment of the
Requirement for the Degree of Doctor of Science in Dentistry

2019

Supervisor of Dissertation

Hyun (Michel) Koo, DDS, PhD

Professor, Department of Orthodontics, Division of Community Oral Health, Division of Pediatric Dentistry

Chair of Dissertation Committee

Evlambia-Harokopakis-Hajishengallis, DMD, DDS, MSc, PhD

Associate Professor of Clinical Pediatric Dentistry

Division Chief of Pediatric Dentistry

Director, Postdoctoral Pediatric Program, Division of Pediatric Dentistry

Dissertation Committee

George Hajieshengallis, DDS, PhD

Thomas W. Evans Centennial Professor, Department of Basic & Translational Science

Jonathon Korostoff, DMD, PhD

Professor of Periodontics

Director, Master of Science in Oral Biology Program

**Dextran-Coated Iron Oxide Nanoparticles as Biomimetic Catalysts
for Biofilm Disruption and Caries Prevention**

Copyright

2019

Yuan Liu

ACKNOWLEDGEMENT

First and foremost, I would like to express my sincere gratitude and appreciation to my mentor, Dr. Hyun Koo. He has been a tremendous mentor for me. I would like to thank him for providing research opportunities, challenging myself all the time and encouraging me to grow as a clinician-scientist. He is a model example of what a mentor and an advisor should be. I cannot thank him enough for helping me realize my academic potential and for preparing myself for an independent research career.

I would like to thank Dr. Evlambia-Harokopakis-Hajishengallis for her generous support throughout my journey at Penn Dental Medicine and taking the position of my Committee Chair. She always provided invaluable guidance not only for my project, but also for my future career as a clinician-scientist in Pediatric Dentistry field. I would also like to thank my committee members, Drs. George Hajishengallis and Jonathon Korostoff, for providing insightful comments and endless encouragement. Their questions and comments encouraged me to think critically and have inspired me to pursue this research in the cariology field.

I could not have done this work without the help from our lab members, Yong Li, Geelsu Hwang, Dongyeop Kim, Yue Huang, Zhi Ren, Hoi-In Jung and Aurea Simon-Soro. These members contributed directly to the work and I really appreciate their time, efforts, encouragement and friendship. I thank Drs. David Cormode, Pratap Naha for providing and characterizing nanoparticles. I also thank Dr. Domenick Zero and his group for analyzing enamel demineralization. Without their precious support, it would not have been possible to conduct this research.

I would like to extend my sincere appreciation to Dr. Dana Graves, who provided me an opportunity to join DScD program and showed consistent guidance.

I would like to thank Colgate-Palmolive Company for providing Fellowship to support my DScD research.

Last but not the least, my special thanks go to my family. Words cannot express how grateful I am to my parents, my husband, my daughter and my parents-in-law for their limitless encouragement, their endless love and support and for believing in me. I could not have achieved anything in my life without them and I am forever in debt for what they have done for me.

This work was supported by National Institute of Health Research Grants, R01-DE025848.

TABLE OF CONTENTS

ABSTRACT

LIST OF ABBREVIATIONS

LIST OF ILLUSTRATIONS

CHAPTER 1 INTRODUCTION

CHAPTER 2 MATERIALS AND METHODS

CHAPTER 3 RESULTS

CHAPTER 4 DISCUSSION

REFERENCES

ABSTRACT

Dextran-coated Iron Oxide Nanoparticles as Biomimetic Catalysts for Biofilm Disruption and Caries Prevention

Yuan Liu

Hyun (Michel) Koo, DDS, PhD

Biofilms are surface-attached bacterial communities embedded within an extracellular matrix that create localized and protected microenvironments. Acidogenic oral biofilms can demineralize the enamel-apatite on teeth, causing dental caries (tooth decay). Current antimicrobials have low efficacy and do not target the protective matrix and acidic pH within the biofilm. Recently, catalytic nanoparticles were shown to disrupt biofilms but lacked a stabilizing coating required for clinical applications. Here, we report dextran-coated iron oxide nanoparticles termed nanozymes (Dex-NZM) that display strong catalytic (peroxidase-like) activity at acidic pH values, target biofilms with high specificity, and prevent severe caries without impacting surrounding oral tissues *in vivo*. Nanoparticle formulations were synthesized with dextran coatings (molecular weights from 1.5 to 40 kDa were used), and their catalytic performance and bioactivity were assessed. We found that 10 kDa dextran coating provided maximal catalytic activity, biofilm uptake, and antibiofilm properties. Surprisingly, dextran coating also enhanced selectivity toward biofilms while avoiding binding to gingival cells. Mechanistic studies indicated that iron oxide cores were the source of catalytic activity, whereas dextran on the nanoparticle surface provided stability without blocking catalysis. Dextran-coating facilitated NZM incorporation into exopolysaccharides (EPS) structure and binding within biofilms, which activated hydrogen peroxide (H₂O₂) for localized bacterial killing and EPS-matrix breakdown. In combination with low concentration of H₂O₂, Dex-NZM inhibited biofilm accumulation on natural teeth in a human-derived *ex vivo* biofilm model, and prevented acid damage of the mineralized tissue. Furthermore,

Dex-NZM/H₂O₂ treatment significantly reduced the onset and severity of caries lesions (vs control or either Dex-NZM or H₂O₂ alone) without adverse effects on gingival tissues or oral microbiota diversity *in vivo*. Therefore, dextran-coated nanozymes have potential as an alternative treatment of a prevalent and costly biofilm-induced oral disease.

LIST OF ABBREVIATIONS

Dex-NZM: dextran-coated nanoenzyme

EPS: exopolysaccharides

MS: mutans streptococci

ECC: early childhood caries

Gtfs: glucosyltransferases

PNs: polymeric nanostructures

TEM: transmission electron microscopy

ICP-OES: inductively coupled plasma optical emission spectroscopy

TMB: 3,3',5,5'-tetramethylbenzidine

NaOAc: sodium acetate

UFTYE: ultra-filtered tryptone-yeast extract

PI: propidium iodide

sHA: saliva-coated hydroxyapatite

CFU: colony forming units

S-ECC: severe early childhood caries

IRB: Institutional Review Board

PBS: phosphate-buffered saline

FISH: fluorescence *in situ* hybridization

SDS: sodium-dodecylsulphate

HE: hematoxylin and eosin

IACUC: University of Pennsylvania Institutional Animal Care and Use Committee

OUT: operational taxonomic units

PCoA: principle coordinate analysis

HGECs: primary human gingival epithelial cells

ANOVA: one-way analysis of variance

EDS: energy dispersive spectroscopy

LIST OF ILLUSTRATIONS

Figure 1. Cariogenic biofilm formation.

Figure 2. Dental plaque architecture: the EPS matrix and spatial organization.

Figure 3. Acidic microenvironments across an EPS-microcolony complex and at the surface of biofilm attachment.

Figure 4. Technological approaches to combat biofilms.

Figure 5. Iron oxide nanoenzyme (NZM).

Figure 6. Optical characterization of Alexa-488 conjugated to Dex-NZM.

Figure 7. Biofilm experimental design and topical treatment regimen.

Figure 8. *Ex vivo* biofilm experimental design and topical treatment regimen.

Figure 9. *In vivo* S-ECC model and topical treatment regimen.

Figure 10. Characterization of Dex-NZM.

Figure 11. Stability and specific binding of Dex-NZM.

Figure 12. Time-lapsed bacterial killing and glucan degradation by Dex-NZM-activated H₂O₂.

Figure 13. Antibiofilm performance of Dex-NZM/H₂O₂.

Figure 14. Antibiofilm properties of topical Dex-NZM/H₂O₂ treatments using an *ex vivo* biofilm model.

Figure 15. Effect of Dex-NZM/H₂O₂ on dental caries *in vivo*.

Figure 16. Effects of topical Dex-NZM/H₂O₂ on oral microbiome and soft tissue *in vivo* after 21 days of treatment.

Figure 17. Schematics of biofilm disruption under acidic condition by catalytic Dex-NZM activation of hydrogen peroxide.

CHAPTER 1: INTRODUCTION

1.1 Oral biofilms: More than Just a Cluster of Bacteria

Many infectious diseases are caused or exacerbated by biofilms¹⁻³. Oral infectious diseases are prime examples of the consequences of dynamic interactions between microorganisms, their host, and the host's diet, leading to microbial colonization of oral surfaces and the establishment of pathogenic biofilms (or dental plaque)^{1,4}. Biofilms are defined as structured communities of microorganisms that are attached to a surface and enmeshed in an extracellular polymeric matrix¹. Advances in DNA- and RNA-sequencing technologies are revealing important information about the diversity in composition, genome content, and behaviors of the biofilm microbiota at different oral sites¹. There are many factors that affect the composition of the microbiota found on various surfaces of the mouth, especially when teeth begin to erupt, providing novel, nonshedding surfaces for colonization by commensals and opportunistic pathogens. These include, but are not limited to, age, diet, oral hygiene, systemic and immune conditions, and the use of certain medications that induce, for example, hyposalivation. The critical role that diet plays in microbial colonization is well illustrated in patients or experimental animals^{5,6}. When hosts are overexposed to dietary sugars, the structure and composition of biofilms formed on teeth changes significantly and the residing microbial communities become highly fit to metabolize carbohydrates and produce acids leading to dental caries⁷.

Although early studies focused on microbial composition of biofilms, it is now clear that microorganisms residing within biofilms are embedded in a matrix containing extracellular polymeric substances such as exopolysaccharides (EPS). The importance of the matrix in the collective microbial behavior and virulence, as well as for tolerance of antimicrobials, is being

increasingly recognized and considered integral to the biofilm lifestyle^{2,3,8}. EPS production directly mediates microbial adherence to a surface and cell-to-cell adhesion, while forming a polymeric matrix that enhances mechanical stability of biofilms. Furthermore, the diffusion-modifying properties of EPS matrix cause chemical/nutrient gradients to form, thereby creating microenvironments within biofilms that can vary widely from other sites in key environmental inputs known to affect microbial behaviors, including pH, redox, and nutrient availability. Thus, the matrix allows the cells to organize into cohesive multicellular ecosystems where cooperative and antagonistic interactions occur within a heterogeneous chemical and physical milieu², helping to create localized niches with differing pathogenic potentials.

1.2 The Cariogenic Biofilm and Its Complex Biochemical Microenvironment

Dental caries is a classic biofilm-induced disease that causes the destruction of the mineralized tooth tissue^{7,9,10}. The microorganisms in the oral cavity are required, but not sufficient, to cause dental caries because the formation of cariogenic biofilms is dependent on the host diet^{1,7,11}. In the mouth, the microbial interactions start with early colonizers that can rapidly adhere to the pellicle-coated tooth surface and then co-adhere with other microorganisms. During this process, the various species interact physically and metabolically to shape the initial biofilm community structure. Certain interactions are beneficial as commensals (e.g., *Streptococcus gordonii* and *Streptococcus salivarius*) can compete against cariogenic bacteria (e.g., *Streptococcus mutans*) by secreting hydrogen peroxide and bacteriocins as “chemical weapons” or counter the deleterious effects of acidification by producing alkali¹¹⁻¹³. However, the dynamic balance between commensals and pathogens can be disrupted by frequent sugar consumption and poor oral care, which promotes the development of virulent biofilms in close proximity to the tooth surface (Figure 1).

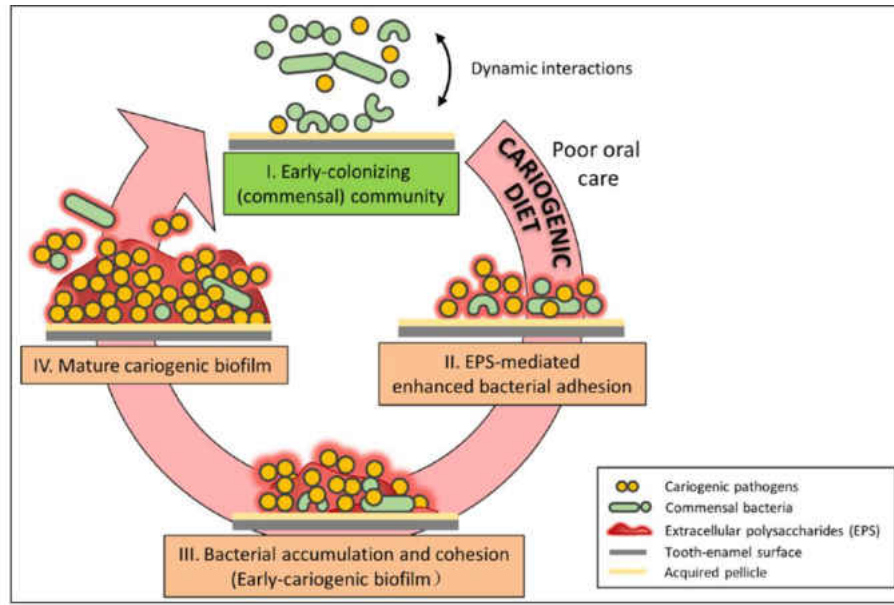


Figure 1. Cariogenic biofilm formation.

A diet rich in sugars fuels the assembly of the EPS matrix and enhances accumulation of acidogenic and acid-tolerant microbiota^{9,10}, which can explain microscopic images of plaque-biofilms collected from caries active sites, revealing bacteria enmeshed in EPS (Figure 2). *S. mutans*, a member of the mutans streptococci (MS) group, has long been implicated with dental caries in human. Extensive clinical, epidemiological, and experimental animal studies have shown, conclusively, though not exclusively, that MS are strongly associated with the disease, especially early childhood caries (ECC)¹⁴. One of the primary adaptations that allow *S. mutans* to become such an efficient opportunistic pathogen within the oral microbiota resides with its exceptional capacity to use a wide variety of carbohydrates to produce EPS and acids, and to live a biofilm lifestyle, including stress resistance and bacterial competence mechanisms^{1,9,10}. One sugar in particular, sucrose, is most cariogenic as the component hexose (glucose and fructose) provide the building blocks of EPS and are efficiently fermented to produce acids¹. When sucrose is available, EPS-producing exoenzymes such as *S. mutans*-derived glucosyltransferases (Gtfs) present in the pellicle and also bound to different microorganisms (including commensal streptococci,

Actinomyces spp., *Candida albicans*) produce large amounts of glucans *in situ*^{15,16}. The surface-formed EPS provide avid binding sites for adhesion and co-adhesion that promote mixed-species biofilm formation¹⁷. EPS then accumulates to form a complex polymeric 3D matrix scaffold in which microorganisms become enmeshed and assemble highly organized and compartmentalized 3D biofilm architecture^{8,15,18}.

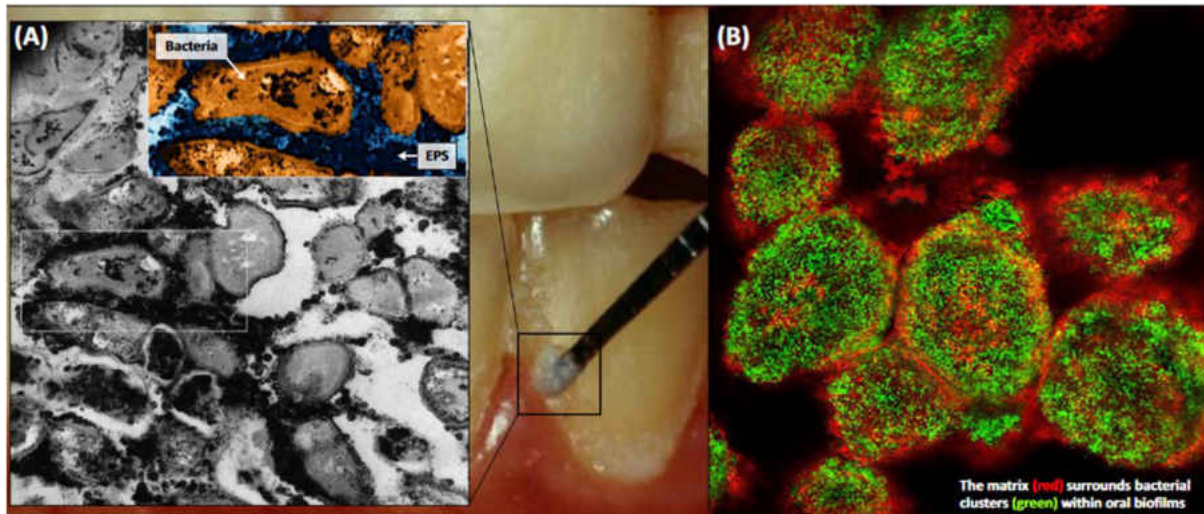


Figure 2. Dental plaque architecture: the EPS matrix and spatial organization. (A) Plaque biofilm from a caries-active subject (photo courtesy of Dr. William Bowen): microscopic image (inset) of plaque-biofilm showing a selected area containing bacterial cells (highlighted in orange) enmeshed in EPS (in dark blue); the image was pseudo-colored using Adobe Photoshop software for visualization purposes (adapted from Hajishengalis et al. 2017). (B) Bacterial clusters (green) surrounded by EPS matrix (red) detected in mature mixed-species oral biofilms formed in sucrose (adapted from Koo and Yamada, 2016).

Biophysical analysis of biofilms and EPS are clarifying their physical contributions to local microenvironments and resistance to mechanical removal and antimicrobials. Well-established biofilms are mechanically difficult to remove from the surfaces and often display viscoelastic properties, which can help them persist by partially yielding rather than detaching when subject to external (fluid) shear stresses^{19,20}. EPS deposition on surfaces and development into polymeric matrix affect the mechanical properties of biofilms, such as increasing adhesive strength to surfaces and coadhesiveness¹⁹. Matrix stiffness appears to increase as the biofilm matures²⁰. The physicochemical properties of the biofilm matrix can also provide protection to embedded bacteria

by reducing drug access and triggering antimicrobial tolerance. For example, the EPS can bind cationic antimicrobials, such as chlorhexidine and antimicrobial peptides, preventing penetration into the deeper layers of the biofilm, and thereby reducing killing efficacy^{21,22}.

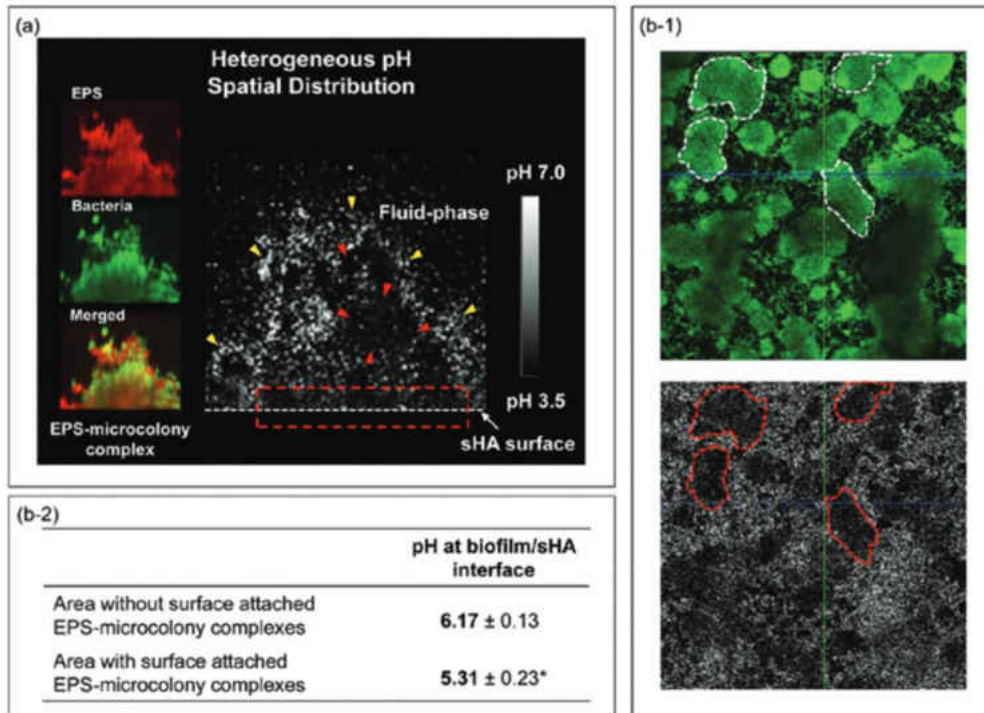


Figure 3. Acidic microenvironments across an EPS-microcolony complex and at the surface of biofilm attachment. Panel (a) gives a detailed image of an EPS-microcolony complex attached to the sHA surface. EPS are depicted in red, bacteria are in green, and dark areas indicate acidic pH, with white areas indicating more neutral pH. The red arrows highlight acidic pH regions within the microcolony structure. Yellow arrows point out pH values close to neutral, which tend to occur at the microcolony/fluid phase interface. The red box denotes acidic pH at the interface between the microcolony complex and the surface of attachment (sHA). Panel (b-1) gives representative cross-sectional images at the sHA surface. White marks indicate the areas with surface-attached microcolonies, while red marks show the corresponding area in the pH channel. The table in Panel (b-2) lists the pH values at the biofilm/sHA interface in areas with and without surface-attached microcolonies following a 30-minute exposure to neutral buffer. The asterisk (*) indicates the values significantly different from each other ($p < .05$). This figure is adapted from Xiao et al.2012.

In the context of dental caries, how and where acidic microenvironments are formed, maintained, and protected within the 3D biofilm architecture may be the key determinant because the buffering saliva surrounding the tooth surfaces is capable of neutralizing acids produced in the mouth. The heterogeneous spatial distribution of pH across oral biofilm structures has been long appreciated⁹.

A fluorescent pH indicator, directly incorporated into the biofilm matrix, revealed a fascinating 3D pH distribution within intact biofilms despite exposure to neutral pH buffer²². Localized low pH environments (4.5-5.5) were detected in the interior of the EPS-microcolony complexes and at the biofilm-apatite interface suggesting that the acids accumulated and confined in these specific areas are not readily neutralized (Figure 3). The EPS matrix has been shown to limit diffusion of charged ions in buffers, whereas uncharged solutes, such as sucrose, can diffuse into biofilms and can be rapidly metabolized into acids by the embedded bacteria²³. Furthermore, extracellular glucans appear to directly trap protons to help retain and accumulate acids within biofilms²⁴. The biofilm matrix can also act as an external digestion system by immobilizing exoenzymes, allowing them to metabolize substrates in close proximity to cells while also participating in matrix remodeling. For instance, soluble fructans and glucans present in the matrix can be degraded by fructanase and dextransase, providing readily fermentable carbohydrates on-site and thereby extending the duration of the acid challenge¹⁵. Thus, EPS can modulate persistent acidification at the tooth interface by helping biofilms to adhere, spatially localize metabolites, and possibly restrict access to buffering saliva, which helps to create a cariogenic microenvironment.

1.3 Challenges and Limitations of Current Antimicrobial Approaches

Despite significant advances in the prevention of dental caries, particularly with the use of fluoride, controlling cariogenic biofilms remains challenging. Major hurdles include the following: 1) microorganisms within biofilms are enmeshed and protected in an EPS-rich matrix, making them difficult to kill or remove; 2) EPS-embedded microbes create highly acidic microenvironments that promote cariogenic biofilm buildup and reduce drug efficacy; and 3) topically applied agents are poorly retained on teeth or within biofilms due to rapid clearance in the mouth. Hence, therapeutic approaches against cariogenic biofilms that could both disrupt the matrix and

simultaneously kill the bacteria within biofilms with enhanced retention and efficacy at acidic pH values would be desirable.

Current approaches against cariogenic biofilms are mostly limited to conventional, broad-spectrum antimicrobials that are incapable of degrading the protective matrix or affecting the physicochemical aspects of dental caries. Although capable of killing planktonic bacteria and reducing microbial accumulation on teeth, chlorhexidine is far less effective against established biofilms, does not prevent caries, and is not suitable for daily use due to adverse effects, including calculus formation and tooth staining²⁵. Likewise, hydrogen peroxide (H₂O₂), a readily available antiseptic agent, also has antimicrobial effects yet limited activity on biofilms even at high concentrations (>3%). Thus, antimicrobials have limited efficacy for caries prevention or treatment if not combined with other modalities. Furthermore, frequent use of broad-spectrum antimicrobials may potentially cause ecological imbalance, increasing susceptibility to reinfection by opportunistic pathogens, including *S. mutans*²⁴. Nevertheless, when conditions are not conducive for dental caries, currently available antimicrobials (including essential oils) can help maintain biofilm accumulation to levels compatible with a healthy mouth²⁶.

Conversely, fluoride is currently the mainstay of caries prevention²⁷, but it does not offer complete protection²⁸. Fluoride exerts its major effect by enhancing remineralization and reducing tooth enamel demineralization but has limited effects against biofilms despite inhibiting bacterial metabolism²⁹. Alternatively, EPS-degrading enzymes like dextranase and mutanase can digest biofilm EPS matrix³⁰ but have no antibacterial activity and limited clinical efficacy when used alone in addition to practical issues, including high cost, immunogenicity and low enzyme stability. Furthermore, natural products have shown multiple biological effects, including antibacterial, antiadhesion, and glucan synthesis inhibition, many of which demonstrated

promising therapeutic effects using *in vivo* caries models³¹. However, it is a challenging approach owing to complex chemistry and composition variability of natural products as well as multistep isolation procedures to derive active compounds, although advances in analytical/chemical separation methods may mitigate these limitations.

Nanomaterials have received increased attention for biofilm control and caries prevention through intrinsic antibacterial properties, as a carrier to deliver bioactive molecules or even as remineralizing agents such as calcium phosphate nanostructures^{32,33}. However, most antibacterial nanomaterials are designed to inhibit bacterial adhesion rather than disrupting existing biofilm. Moreover, these materials are not designed to break down the biofilm matrix or to specifically target the pathological microenvironments found in cariogenic biofilms (with few exceptions). Therefore, new approaches for enhanced anticaries effects should eradicate biofilms locally and, at the same time, prevent acid dissolution of the adjacent tooth enamel.

1.4 New Therapeutic Approaches for Biofilm Control

While our understanding of biofilm microenvironments is evolving, technological advances are providing unprecedented avenues to develop multi-targeted therapeutic approaches that prevent and disrupt biofilms or enhance drug efficacy. Nano- and chemical engineering approaches provide unparalleled flexibility to control the composition, size, shape, surface area and surface chemistry, and functionality of nanostructures that can be used to develop a new generation of modified materials or to coat existing solid surfaces to prevent the formation of biofilms (Figure 4). Functionalized nanoparticles, including stimuli-triggered activation, can be designed to enhance penetration and selectively target or release drugs locally after bacterial attachment or within biofilms. For example, nanoparticles can be used to coat existing surfaces (e.g., teeth) and exogenously introduced surfaces (e.g., restorative or implant materials) for prevention of bacterial

adhesion and cariogenic biofilm formation³⁴. Specifically, functionalized nanoparticles can be conceived to carry and selectively release or activate antimicrobial agents at the surface of attachment or within oral biofilms. The latter mechanism includes “smart release or activation” of agents when triggered by pathogenic microenvironments (e.g., acidic pH) that could simultaneously kill bacteria and dismantle the biofilm matrix. Recently, functional polymeric

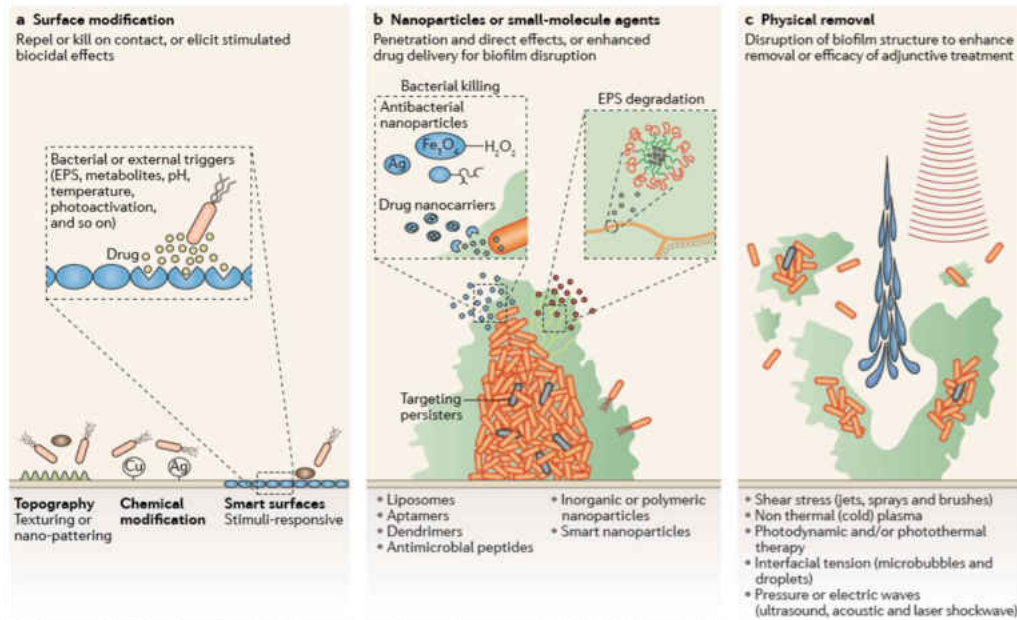


Figure 4. Technological approaches to combat biofilms. Recent advances in material science and nanotechnology have enabled the engineering of a wide range of biofilm-targeting strategies. a | The material and surface properties of medical devices, such as surface charge, hydrophobicity, roughness, topography and chemistry, among others, can be modified to prevent bacterial attachment and thus attenuate or block biofilm formation. In addition, ‘smart’ or stimuli-triggered responsive surfaces can be constructed that elicit their effect only in response to physical contact with cell wall-associated or membrane-associated adhesins or bacterial chemical cues (such as secreted extracellular polymeric substance (EPS) and metabolites) or external triggers (such as photoactivation or pH). b | Advances in nanoparticle synthesis have led to the development of diverse approaches to combat biofilms. c | New technologies for physical biofilm removal, including mechanical, energy-based and light-based disruption, may further improve biofilm intervention strategies. This figure is adapted from Koo et al.2018 with permission.

nanostructures (PNs) were developed for enhanced drug delivery when triggered by acidic pH values³⁵. These nanostructures are formed from diblock copolymers and 2-propylacrylic acid that self-assemble into cationic nanoparticles. By tuning the PNs’ outer corona surface, they display outstanding adsorption affinities to pellicle and EPS-coated apatitic surfaces due to strong electrostatic interaction³⁵. Owing to hydrophobic cores, these “nanocarriers” can encapsulate

nonpolar antibacterial drugs such as farnesol with high efficiency while making them soluble in aqueous solution due to hydrophilic outer corona. With this specific polymer conjugation, the nanoparticles undergo core destabilization and drug release in a pH-responsive manner, triggered by the acidification of the biofilm microenvironment in cariogenic conditions. These pH-activated polymeric nanocarriers enhanced the antibiofilm activity of farnesol by 4-fold (vs. free farnesol), significantly improving its efficacy against caries severity *in vivo* (>10-fold) under twice-daily topical treatment regimen.

Iron oxide nanoparticles have been widely used as contrast agents in MRI because of their high biocompatibility and ability to penetrate tumor and atherosclerotic plaque, resulting in many FDA-approved formulations³⁶. Interestingly, the iron oxide nanoparticles display an intriguing biomimetic activity by displaying enzyme-like (peroxidase) activity, and thereby have been termed nanocatalysts or nanozymes. In a seminal work, Gao et al.³⁷ demonstrated that iron oxide

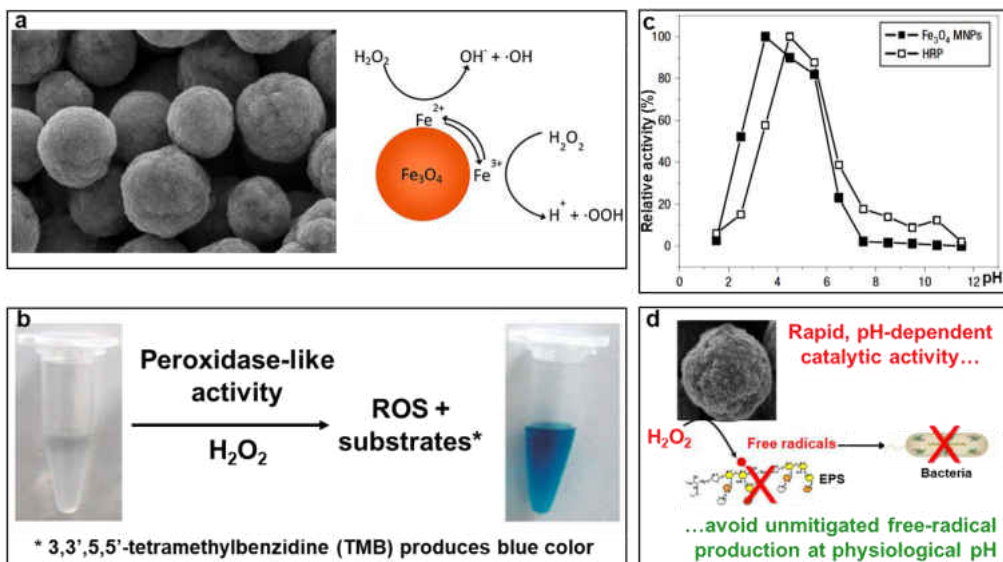


Figure 5. Iron oxide nanoenzyme (NZM). (a) SEM image iron oxide nanoenzymes and the mechanism by which NZM catalyzes free radical generation in the presence of H_2O_2 . (b) Demonstrating the catalytic activity of NZM via colorimetric reaction by using 3,3,5,5-tetramethylbenzidine (TMB) as a substrate which produces a blue color after reacting with the free radicals catalyzed by nanoparticles in the presence of H_2O_2 . (c) This catalytic activity is rapid and pH dependent activity. (d) The free radicals can kill bacteria and degrade EPS (Gao et al. 2007).

nanoenzyme (NZM) possess an intrinsic peroxidase-like activity, which enable them to catalyze the breakdown of H_2O_2 , and rapid production of bioactive free radicals (Figure 5). Hydrogen peroxide (H_2O_2) is a commonly used low cost antiseptic for general disinfection purposes or as tooth-whitening agent (at concentrations as high as 10%) because it generates free radicals that exhibit antibacterial activity or stain removal (through degradation of polymeric substances). However, the process is slow and H_2O_2 by itself has modest anti-biofilm or endodontic disinfection effects when used alone. The catalytic nanoparticles could potentiate the efficacy of hydrogen peroxide by enhancing the production of free radicals locally for improved antibacterial effects. Recently, this concept was proven successful to kill bacterial embedded within biofilms using short-term topical applications with exceptional efficacy (5,000 times more effective than H_2O_2 alone)³⁷. However, for clinical applications, NZM require coatings as uncoated nanoparticles lack stability in physiological media and in solutions suitable for therapeutic formulations and can bind to biological tissues indiscriminately, which could lead to adverse effects to healthy tissues^{38,39}. Ideally, the presence of coatings would improve biofilm targeting and maintain catalytic activity, while enhancing biocompatibility, which could result in a more practical and specific anti-biofilm treatment.

In this study, we hypothesized that dextran-coated NZM (Dex-NZM) could be incorporated into biofilms while maintaining its intrinsic catalytic activity to break down the EPS structure and kill bacteria upon exposure to H_2O_2 at cariogenic (acidic) pH values. In addition, dextran coating would also result in stability in aqueous formulations and enhanced biofilm targeting specificity, providing biocompatibility to the host soft tissue in the oral cavity.

CHAPTER 2: MATERIALS AND METHODS

2.1 Synthesis of Dextran-Coated NZM (Dex-NZM)

A range of Dex-NZM formulations were synthesized based on a protocol published elsewhere^{40,41}, using varying dextran molecular weights (from 1.5 to 40 kDa). In brief, 12.5 g of dextran (Pharmacosmos, Holbaek, Denmark) of the selected molecular weight was dissolved in 25 mL of deionized (DI) water. Once the dextran completely dissolved in DI water, the solution was placed in an ice bath and purged with nitrogen gas to remove oxygen from the flask. A 0.985 g portion of ferric chloride hexahydrate and 0.366 g of ferrous chloride tetrahydrate (Sigma-Aldrich, St. Louis, MO) were each dissolved in 6.25 mL of DI water separately and then added to the dextran solution. The reaction mixture was allowed to stir for 45 min at 4°C for complete mixing of iron salts with dextran solution. Next, 15 mL of ammonium hydroxide (28–30%, Sigma-Aldrich) was added to the reaction mixture using a syringe pump. The ammonium hydroxide was added to the reaction mixture at different rates, i.e., 0.3 $\mu\text{L}/\text{min}$ for the first 2.5 h and then 0.6, 0.9, and 1.2 $\mu\text{L}/\text{min}$ for 1 h each consecutively. The remainder of the ammonium hydroxide was added to the reaction mixture at a rate of 4 $\mu\text{L}/\text{min}$. After the addition of ammonium hydroxide was completed, the reaction mixture was heated to 90°C for 1 h and then stirred overnight at room temperature. The nanoparticle suspension was then spun at 20,000 g for 30 min at 4°C, after which the supernatant was collected and concentrated using ultrafiltration tubes (molecular weight cut off 100 kDa, Sartorius Stedim Biotech, Germany). The concentrated Dex-NZM was purified with citrate buffer via diafiltration columns (100 kDa, Spectrum Labs, CA). After purification, Dex-NZM was stored at 4°C. Conjugation with Alexa 488 NHS Ester (ThermoFisher Scientific) was achieved by introducing amine groups to the dextran coating, as previously described⁴¹, and then following the manufacturer's instructions. These fluorescent nanoparticles were further purified using

ultrafiltration tubes (molecular weight cut off 100 kDa, Sartorius Stedim Biotech). UV-vis (Evolution 201 UV-vis spectrophotometer, ThermoFisher Scientific) and fluorescence spectra (SpectraMax, M5, Molecular Devices) proved that Alexa-488 was conjugated successfully to the nanoparticle surface (Figure 6). Uncoated NZM were synthesized by first dissolving 1.1 g of ferric chloride hexahydrate and 0.4 g of ferrous chloride tetrahydrate (Sigma-Aldrich) in 15 mL of DI water each and then transferring these solutions to a three-necked flask. The reaction mixture was stirred under an inert nitrogen atmosphere. The reaction mixture was heated to 85°C, and then 20 mL of diluted ammonium hydroxide solution (2.5 mL of 28% ammonium hydroxide diluted to 20 mL with DI water) was added dropwise to the reaction mixture. After addition of ammonium hydroxide, the reaction mixture was stirred at 85°C for 1 h. Next, the nanoparticles were collected magnetically and were purified with DI water using diafiltration columns (100 kDa)⁴².

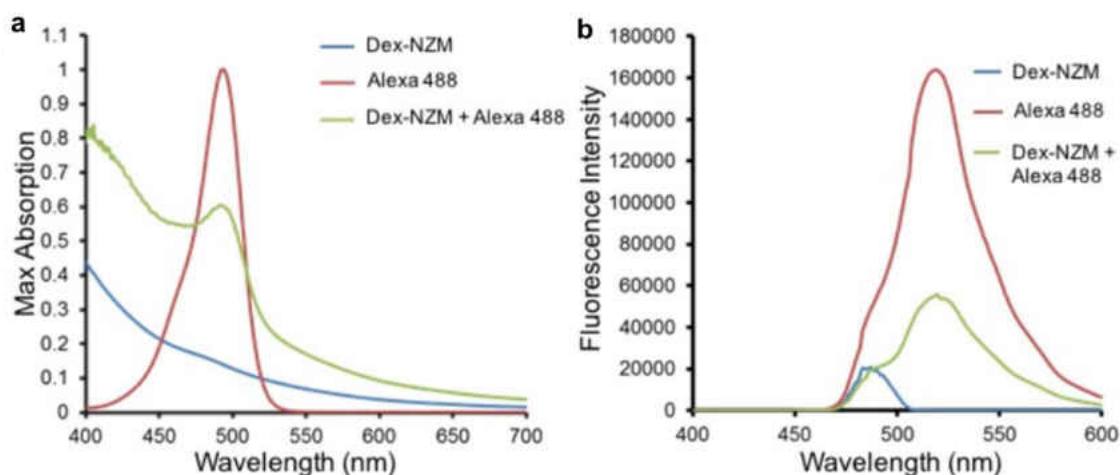


Figure 6. Optical characterization of Alexa-488 conjugated to Dex-NZM. a) UV-visible spectra and b) emission spectra of Dex-NZM, Alexa-488 and Alexa-488 conjugated Dex-NZM.

2.2. Characterization of Dex-NZM

Hydrodynamic Diameter and Zeta Potential. The hydrodynamic diameter and zeta potential of each Dex-NZM were measured using a Nano-ZS 90 (Malvern Instrument, Malvern, UK). Then

1.5 and 1 mL of diluted Dex-NZM (12.5 μ L Dex-NZM stock solution to 1 mL of DI water) were used for the hydrodynamic diameter and zeta potential measurements, respectively.

Transmission Electron Microscopy. Transmission electron microscopy (TEM) of each Dex-NZM was performed using a JEOL 1010 microscope operating at 80 kV. Then 5 μ L of nanoparticle suspension was dropped onto the TEM grid (FCF-200-Cu, Electron Microscopy Sciences, Hatfield, PA), and the liquid was allowed to dry before microscopy was performed.

Inductively Coupled Plasma Optical Emission Spectroscopy. The iron concentration in each Dex-NZM formulation was measured using inductively coupled plasma optical emission spectroscopy (ICP-OES)⁴¹. Then 5, 10, or 25 μ L of Dex-NZM was dissolved in 1 mL of aqua regia. After complete dissolution of Dex-NZM, the final volume in each tube was adjusted to 10 mL with DI water. The iron concentration was measured using ICP-OES (Spectro Genesis ICP). The concentration obtained from the ICP-OES was adjusted by the dilution factor for each sample and then averaged to determine the iron concentration in the stock solution. The total amount of iron within intact biofilms (i.e., bacterial cells and EPS combined) was also measured using ICP-OES. Biofilms treated with Dex-NZM formulations were transferred to glass tubes and digested with 1 mL of aqua regia overnight at room temperature. Then the volume was adjusted to 10 mL with DI water prior to analysis with ICP-OES^{37,41}. Three independent experiments were performed for each Dex-NZM formulation, and the data are presented as mean \pm SD.

Catalytic Activity (TMB) Assay. The peroxidase-like catalytic activities of the Dex-NZM formulations were investigated via a colorimetric assay using 3,3',5,5'-tetramethylbenzidine (TMB, Sigma Aldrich) and hydrogen peroxide (H_2O_2) following a previously published protocol³⁷, with a slight modification. This assay is well established as an assessment of peroxidase-like activity^{43,44}, where H_2O_2 and the TMB substrate are converted to water and an oxidized form of

TMB that is blue in color. UV measurements at 652 nm allow the oxidation of TMB to be monitored and catalytic activity to be compared. The catalytic activity of each Dex-NZM was measured at three different pH values, i.e., 4.5, 5.5, and 6.5. The assay was performed in 96-well plates. A 300 μ L portion of 0.1 M sodium acetate (NaOAc) buffer at the appropriate pH was added to each well of a 96-well plate. Then, 1.2 μ L of Dex-NZM (5 mg Fe/mL) was added to the wells. After the addition of Dex-NZM, 3 μ L TMB (10 mg/mL) and 15 μ L of H₂O₂ (0.5% v/v) were added to each well and mixed vigorously. After addition of hydrogen peroxide, the 96 well plate was immediately placed into a plate reader, and the absorbance was recorded at 652 nm at 1 min intervals for 30 min. Three independent experiments were performed for each Dex-NZM formulation. The slope of the line was calculated and averaged, and the data are presented as mean \pm SD.

Iron Release and Catalytic Activity of Released Iron Ions. The effect of iron ion release from 10 kDa Dex-NZM was studied in 0.1 M NaOAc buffer (pH 4.5). A 1 mL portion of Dex-NZM (5 mg Fe/ml) was diluted with 9 mL of 0.1 M NaOAc buffer. After mixing, samples were incubated at 37°C for 5, 30, 60, and 120 min (n = 3 per time point). After the desired incubation time, the free iron ions and nanoparticles were separated using ultrafiltration tubes (10 kDa MWCO). The iron content in the filtrate and the nanoparticle pellet from each incubation time point were measured using ICP-OES. The catalytic activity of the released iron in the supernatant and nanoparticle pellet from each incubation time point was analyzed using the TMB assay, as described above. Three independent experiments were performed per incubation time point, and the data are presented as mean \pm SD.

Dex-NZM Binding to Saliva-Coated Hydroxyapatite Beads. In this binding assay, 10 mg of saliva-coated HA beads was incubated in 500 μ L of Dex-NZM solution at a concentration of 0.2 mg/mL

for 30 min with rocking at 37°C. Then the supernatant was removed, and the beads were washed three times with water to remove unbound nanoparticles. The beads were dissolved with 1 mL of 70% HNO₃, and the iron was analyzed via ICP-OES⁴¹.

2.3 Bacterial Killing and EPS Degradation by Dex-NZM activated H₂O₂

Time-lapse high-resolution confocal fluorescence imaging was performed to assess the dynamics of bacterial killing and glucan structure breakdown. *Streptococcus mutans* UA159 (ATCC 700610), a virulent cariogenic pathogen and well-characterized biofilm-forming strain, was grown in ultra-filtered (10-kDa cutoff; Millipore) tryptone-yeast extract (UFTYE) broth at 37°C and 5% CO₂ to mid-exponential phase. Dex-NZM was added to actively growing *S. mutans* (10⁸ CFU/mL) at a concentration of 1 mg/mL in the presence of 1% H₂O₂ at pH 4.5 or pH 6.5. SYTO 60 (652/678 nm; Molecular Probes) and propidium iodide (PI, 535/617 nm; Molecular Probes) were used for labelling live and dead cells. In addition, we conjugated Dex-NZM with Alexa Fluor 488 (490/525 nm; Molecular Probes) to visualize nanoparticle binding and localization on the cell surface. Confocal images were acquired in the same field of view at 0, 10, 20, 30, and 40 min using Zeiss LSM800 upright single photon laser scanning microscope with a 40 × (numerical aperture, 1.2) water immersion objective. Images were analyzed by ImageJ. For EPS degradation, insoluble glucans were produced by purified *S. mutans*-derived exoenzyme glucosyltransferase B (GtfB) immobilized on poly-L-lysine coated MatTek dish and labelled with 1 μM Alexa Fluor 647-dextran conjugate (647/668 nm; Molecular Probes) as described previously⁴⁵. The preformed fluorescently labelled glucans were then incubated with Dex-NZM (1 mg/mL) and 1% H₂O₂ (in 0.1 M NaOAc buffer at pH 4.5 or 6.5), and time-lapsed confocal imaging was performed as described above using a 20 × (numerical aperture, 1.0) water immersion objective. To further examine the glucan degradation process, we also employed computational analysis (Amira and

ImageJ) that generates structural scaffold based on geometrical and topological properties of the EPS, including length and width⁴⁵.

2.4 Oral Biofilm Model

Biofilms were formed on saliva-coated hydroxyapatite (sHA) disks (surface area, $2.7 \pm 0.2 \text{ cm}^2$, Clarkson Chromatography Products Inc., South Williamsport, PA), as described elsewhere^{22,37}, that were vertically suspended in 24-well plates. *Streptococcus mutans* UA159 (ATCC 700610) was grown in ultrafiltered (10 kDa molecular-mass cutoff) tryptone-yeast extract broth (UFTYE; 2.5% tryptone and 1.5% yeast extract) containing 1% (w/v) glucose at 37°C and 5% CO₂ to mid-exponential phase. Each HA disk was coated with filter-sterilized saliva for 1 h at 37°C (the saliva was prepared as described previously)^{22,37}. These sHA disks were each inoculated with $\sim 2 \times 10^5$ colony forming units (CFU) of *S. mutans* per milliliter in UFTYE culture medium (pH 7.0) containing 1% (w/v) sucrose at 37°C. The culture medium was changed twice daily (at 19 and 29 h) until the end of the experimental period (43 h). The biofilms were collected and analyzed for Dex-NZM binding and catalytic activity as well as bioactivity as described below.

Bacterial Killing and Biomass Reduction by Dex-NZM with H₂O₂. To assess the antibiofilm effect of Dex-NZM bound within biofilms, the sHA disks and biofilms were topically treated twice daily by placing them in 2.8 mL of Dex-NZM (0.5 mg/mL) in 0.1 M NaOAc (pH 4.5) or vehicle control (buffer only) for 10 min at room temperature at specific time points (Figure 7). At the end of the experiment (43 h), the Dex-NZM- and vehicle-treated biofilms were placed in 2.8 mL of H₂O₂ (1%, v/v or buffer) for 5 min. After H₂O₂ exposure, the biofilms were washed with sterile saline solution (0.89% NaCl) three times. The biofilms were then removed by a spatula from sHA discs and homogenized via bath sonication followed by probe sonication^{35,37,46}. Samples of these biofilm suspensions were serially diluted and plated onto blood agar plates using an automated EddyJet

Spiral Plater (IUL, SA, Barcelona, Spain). The numbers of viable cells in each biofilm were calculated by counting CFU. The remaining suspension was centrifuged at 5,500 g for 10 min, the resulting cell pellets were washed twice with water, oven-dried for 2 h, and weighed^{35,37,46}.

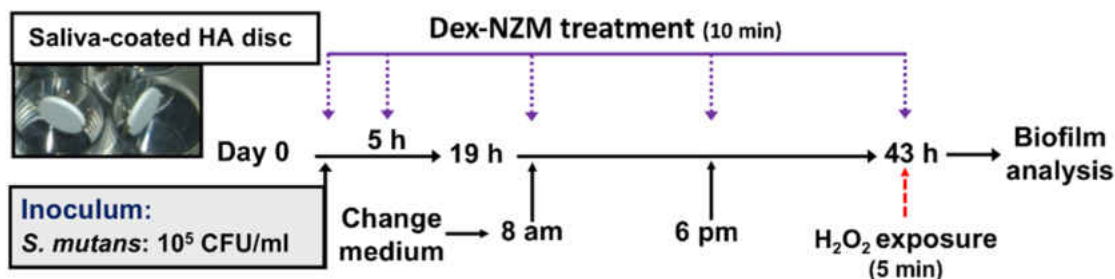


Figure 7. Biofilm experimental design and topical treatment regimen. For assessment of Dex-NZM binding, bacteria killing effect and catalytic activity, the biofilms were exposed to Dex-NZM at 1 pm, 6 pm (day 1), and 8 am and 6 pm (day 2). At the end of experimental period (43 h), the analyses were conducted.

Catalytic Activity within Intact Biofilm. The catalytic activity of 10 kDa Dex-NZM within intact biofilms was measured after incubations similar to those described above. Biofilms grown on sHA disks were treated twice daily by placing them in 2.8 mL of Dex-NZM (0.5 mg/mL) in 0.1 M NaOAc (pH 4.5) or vehicle control (buffer only) for 10 min at room temperature at specific time points (Figure 7)³⁷. At the end of the experimental period (43 h), all the biofilms were washed with 0.1 M NaOAc buffer (pH 4.5) three times and transferred to the reaction buffer (500 μ L 0.1 M NaOAc, pH 4.5 containing 1% H₂O₂ and 100 μ g TMB). The reaction was allowed to proceed for 30 min at room temperature without shaking. After the reaction, still images of intact biofilms were acquired, and subsequently, the biofilms were removed using a spatula from the disk surfaces and centrifuged at 5,500 g for 10 min. Then the absorbance from the supernatant was recorded at 652 nm. Three independent experiments were performed, and the data are presented as mean \pm SD.

Distribution of Dex-NZM within Biofilm Architecture. Confocal fluorescence imaging was performed using an upright microscope (LSM 800, Zeiss) with a 20 \times (numerical aperture, 1.0) water immersion objective to assess the distribution of Dex-NZM, dynamics of bacterial killing, and EPS degradation within biofilm. Dex-NZM conjugated with Alexa Fluor 488, prepared as

described above, was used. SYTO 82 (541/560 nm; Molecular Probes) was used for labeling bacteria, and Alexa Fluor 647-dextran conjugate (647/668 nm; Molecular Probes) was used for labeling insoluble EPS. Each component was illuminated sequentially to minimize cross-talk as follows: Alexa 488 (Dex-NZM) was excited using 488 nm and was collected by a 480/40 nm emission filter; SYTO 82 (bacterial cells) was excited using 560 nm, and was collected by a 560/40 nm emission filter; Alexa 647 (EPS) was excited using 640 nm and was collected by a 670/40 nm emission filter. To assess colocalization of Dex-NZM with bacteria or EPS, each channel was processed with Otsu's thresholding method using ImageJ.

2.5 Human-derived *Ex Vivo* Biofilm Model on Natural Teeth

To further assess the antibiofilm efficacy of Dex-NZM-mediated H₂O₂ catalysis, we examined whether daily topical treatments can disrupt cariogenic biofilm development and prevent enamel surface damage using an *ex vivo* biofilm model. Plaque-biofilm samples were collected from children (age between 36 and 72 months) diagnosed with severe early childhood caries (S-ECC) as defined by the 2014 Conference Manual of the American Academy of Pediatric Dentistry. Ethical approval of the study and the written consent/permission forms were obtained from Institutional Review Board (IRB) at University of Pennsylvania (IRB 824243) prior to the study commencement. For each child, written permission form was reviewed and signed by their legal guardians. Pooled plaque samples were collected from the available smooth tooth surfaces using a sterilized periodontal scaler and transferred into 1 mL phosphate-buffered saline (PBS) in a sterilized Eppendorf tube. After collection, the plaque samples were immediately transported on ice to the laboratory, and then gently vortexed and sonicated (three 10 s pulses with 30 s intervals at 7 W) to disperse the aggregates before inoculation^{47,48}. Different pooled samples were checked for *S. mutans*, which is frequently found in high numbers in cariogenic plaque-biofilm associated

with S-ECC¹⁴, and total cultivable bacteria to ensure similar *S. mutans* proportion for the inoculum. The human-derived *ex vivo* biofilms were formed on sterilized human enamel blocks (4 mm × 4 mm) mounted vertically in 24-well plates using a custom-made wire holder (Figure 8). Each enamel block was inoculated with homogenized pooled plaque in UFTYE containing 1% sucrose at 37°C and 5% CO₂ for 115 h (5 d) as described previously²². To mimic topical treatment regimen, the enamel blocks and biofilms were topically treated twice-daily by placing them in 2.8 ml of Dex-NZM (1 mg/mL) in 0.1 M NaOAc (pH 4.5) for 10 min immediately followed by 1% H₂O₂ exposure for 5 min. After each treatment, the biofilms were dip-washed with 0.89% NaCl and transferred to fresh culture medium. Biofilm were removed at 115 h for three-dimensional (3D) structural analysis and the enamel blocks were collected for surface analysis via surface topography, roughness measurement and transversal microradiography^{48,49}.

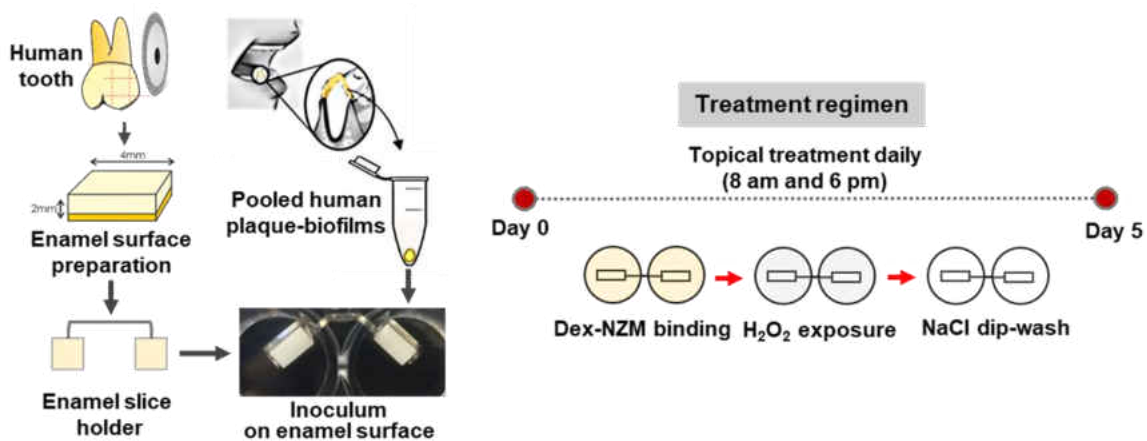


Figure 8. *Ex vivo* biofilm experimental design and topical treatment regimen.

Analysis of Ex Vivo Derived Biofilm. The biofilms formed on enamel blocks were gently washed twice with PBS and fixed with 4% paraformaldehyde (in PBS, pH7.4) at 4°C for 4 h. After fixation, the biofilms were washed twice with PBS, then transferred into 50% ethanol (in PBS, pH 7.4) and stored at -20°C. The biofilm 3D architecture was analyzed via fluorescence *in situ* hybridization (FISH) as detailed previously⁴⁸⁻⁵¹. FISH oligonucleotide probes used in this study were: EUB338,

5'-GCTGCTCCCGTAGGATG-3' with Cy3 for all bacteria; Smu587, 5'-ACTCCAGACTTTCCTGAC-3' with Alexa Fluor 488 for *S. mutans*. The sample in the hybridization buffer (30% formamide, 0.9 M NaCl, 0.01% sodium-dodecylsulphate (SDS), 20 mM Tris-HCl, pH 7.2) with the probes was incubated at 46°C for 2 h. After incubation, the hybridized cells were washed with washing buffer (0.2 M NaCl, 20 mM Tris-HCl (pH 7.5) and 5 mM EDTA, 0.01% SDS), and further incubated at 46°C for 10 min⁴⁸⁻⁵¹. The EPS were labeled with 1 µM Alexa Fluor 647-dextran conjugate (647/668 nm; Molecular Probes)²². The 3D biofilm architecture was acquired using Zeiss LSM 800 with a 20 × (numerical aperture, 1.0) water immersion objective. The biofilms were sequentially scanned using diode lasers (488, 561, and 640 nm), and the fluorescence emitted was collected with GaAsP or multi-alkali PMT detector (475–525 nm for Alexa Fluor 488, 540–580 nm for Cy3, and 645–680 nm for Alexa Fluor 647-dextran conjugates, respectively). Amira 5.4.1 software (Visage Imaging) was used to create 3D renderings to visualize the architecture of the biofilms.

Enamel Surface Analyses. The surface topography and roughness of the tooth-enamel surface (after biofilm removal) were analyzed by a nondestructive confocal contrasting method using Zeiss LSM 800 with a C Epiplan-Apochromat 50 × (numerical aperture, 0.95) nonimmersion objective. The images were processed using ConfoMap (Zeiss) to create 3D topography rendering and measure the surface properties in 3D. After surface analyses, enamel blocks were mounted on plastic rods and sectioned with a hard tissue microtome (Silverstone-Taylor Hard Tissue Microtome, Series 1000 Deluxe) for transversal microradiography. One 100 µm section was obtained from the center of each specimen, mounted on X-ray sensitive plates (Microchrome Technology) and subjected to X-ray, along with an aluminum step wedge. Microradiographic

images were analyzed with Inspektor TMR 2000 software (ver. 1.25) with sound enamel defined at 87% mineral volume to obtain mean lesion depth (μm)⁴⁹.

2.6 *In Vivo* Rodent Model of Severe Childhood Caries

The therapeutic efficacy of Dex-NZM-mediated H_2O_2 catalysis were assessed on a well-established rodent caries model as detailed elsewhere^{35,52}. Briefly, 15 days-old female Sprague–Dawley rat pups were purchased with their dams from Harlan Laboratories (Madison). Upon arrival, animals were screened for *S. mutans* and were determined not to be infected with the pathogen by plating oral swabs on mitis salivarius agar plus bacitracin. The animals were then infected by mouth with actively growing (mid-logarithmic) culture of *S. mutans* UA159, and their infections were confirmed at 21 days via oral swabbing. To simulate clinical situation, we developed a combination therapy consisting of 1 min topical treatment of Dex-NZM at 1 mg/mL (or buffer) immediately followed by 1% H_2O_2 (or buffer) exposure. All the pups (equal numbers) were randomly placed into treatment groups, and their teeth were treated topically twice daily using a custom-made applicator (Figure 9)^{35,37}. The treatment groups were: (1) control (0.1 M NaOAc buffer, pH 4.5), (2) Dex-NZM only (1 mg/mL), (3) 1% H_2O_2 only, and (4) Dex-NZM/ H_2O_2 (1 mg/mL Dex-NZM with 1% H_2O_2). The treatments were blinded by placing the test agents in color-coded vials. Each group was provided the National Institutes of Health cariogenic diet 2000 and 5% sucrose water ad libitum. The experiment proceeded for 3 weeks (21 days). All animals were weighed weekly, and their physical appearances were noted daily. At the end of the experimental period, the animals were sacrificed, and the jaws were surgically removed and aseptically dissected, followed by sonication to recover total oral microbiota⁵³. All jaws were defleshed and the teeth were prepared for caries scoring according to Larson's modification of Keyes's system^{35,37,52}. Determination of caries score of the jaws was performed by a calibrated

examiner who was blind for the study by using codified samples. Furthermore, both gingival and palatal tissues were collected and processed for hematoxylin and eosin (HE) staining for histopathological analysis by an oral pathologist at Penn Oral Pathology. This study was reviewed and approved by the University of Pennsylvania Institutional Animal Care and Use Committee (IACUC #805529).

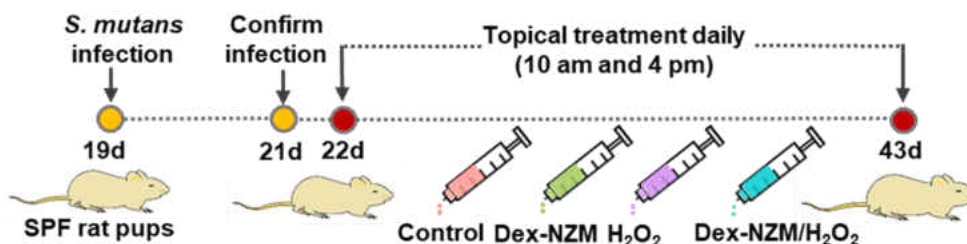


Figure 9. *In vivo* S-ECC model and topical treatment regimen. In this model, tooth-enamel progressively develop caries lesions (analogous to those observed in humans), proceeding from initial areas of demineralization to moderate lesions and onto extensive (severe) lesions characterized by enamel structure damage and cavitation.

16S rRNA Gene Amplicon Sequencing. Dispersed oral microbiota samples were eluted in PBS with cell lysis buffer from a DNeasy kit (Qiagen) as described by the manufacturer. After a 60 s vortex, DNA present in the buffer was isolated with the DNeasy Power Soil HTP kit and quantitated with a spectrophotometer (Tecan). The 27F/338R primer with Golay-barcode in the reverse primer was used to amplify the V1–V2 region of 16S ribosomal DNA (16S rDNA; IDT). Four replicate PCR reactions were performed for each sample using Q5 Hot Start High Fidelity DNA Polymerase (New England BioLabs). Each PCR reaction contained: 4.3 μ L microbial DNA-free water, 5 μ L 5 \times buffer, 0.5 μ L dNTPs (10 mM), 0.17 μ L Q5 Hot Start Polymerase, 6.25 μ L each primer (2 μ M), and 2.5 μ L DNA. PCR reactions without template or with synthetic DNAs were performed as negative and positive controls, respectively. PCR amplification was done on a Mastercycler Nexus Gradient (Eppendorf) using the following conditions: DNA denaturation at 98°C for 1 min, then 20 cycles of denaturation 98°C for 10 s, annealing 56°C for 20 s and extension 72°C for 20 s, last

extension at 72°C for 8 min. PCR replicates were pooled and then purified using a 1:1 ratio of Agencourt AMPure XP beads (Beckman Coulter), following the manufacturer's protocol. The final library was prepared by pooling 10 µg of amplified DNA per sample. Those that did not reach at the DNA concentration threshold (e.g., negative control samples) were incorporated to the final pool by adding 12 µL. The library was sequenced to obtain 2 × 250 bp paired-end reads using the MiSeq Illumina⁵⁴. Sequence data was analyzed with the QIIME pipeline (ver. 1.9.1)⁵⁴. The forward and reverse reads were joined with no mismatches permitted. Read quality lower than Q29 or more than 3 consecutive low-quality base calls were discarded. Sequences were clustered into operational taxonomic units (OTU) at a 97% similarity threshold using the UCLUST method⁵⁵. Taxonomic assignments were obtained based on GreenGenes16S rRNA gene database⁵⁶. To test the differences between communities, library vegan, and Unifrac distances were used^{57,58}. Diversity, richness, and bacterial taxon abundances were compared using the Wilcoxon rank sum test. Principle coordinate analysis (PCoA) was performed using library APE for R programming language⁵⁹.

2.7 Cell Viability

The cytotoxicity of each Dex-NZM formulation was evaluated in primary human gingival epithelial cells (HGECs) and human fibroblast (BJ-5ta) cells using the MTS [(3-(4,5-dimethylthiazol-2-yl)-5-(3-carboxymethoxyphenyl)-2-(4-sulfophenyl)-2H-tetrazolium)] assay (CellTiter 96 cell proliferation assay kit; Promega, WI, USA)⁶⁰. HGECs were a gift from Dr. Manju Benakanakere (School of Dental Medicine, University of Pennsylvania), and BJ-5ta cells were purchased from ATCC (Manassas, VA, USA). HGECs were cultured in keratinocyte serum-free medium (Invitrogen, NY)⁶¹. BJ-5ta cells were cultured in a 4:1 mixture of Dulbecco's Modified Eagle's Medium (DMEM) and medium 199, supplemented with 10% fetal bovine serum

(Gibco, NY) and 0.01 mg/mL of hygromycin B (Sigma-Aldrich). The assay was performed in 96-well plates; 10,000 cells in 100 μ L of cell culture media were added to each well, and then the plates were incubated at 37°C in a 5% CO₂ atmosphere for 24 h. After this time, the cells were washed gently with sterile phosphate buffered saline (PBS) before 100 μ L of Dex-NZM or uncoated NZM (0.5 mg Fe/mL) in cell culture medium was added to the wells. The plates were then incubated at 37°C in 5% CO₂ atmosphere for 10 min. After this incubation, the media was removed, the cells were washed with PBS, and then 20 μ L MTS reagent and 100 μ L cell culture medium were added to each well. The plates were then incubated at 37°C in a 5% CO₂ atmosphere for 1 h, after which time the absorbance was recorded at 490 nm using a plate reader. For the 24 h cell viability experiment, the cell culture medium with Dex-NZM was removed from each well after 10 min of incubation. Then the cells were washed with PBS, 100 μ L of fresh cell culture medium was added to each well, and the plates incubated for a further 24 h. The MTS reagents were then added, and the absorbance was recorded at 490 nm (as described above). Three independent experiments were performed for each Dex-NZM formulation. The percentage of cell viability was calculated, and the results were presented as mean \pm SD.

2.8 Statistical Analysis

All the results are presented as mean \pm SD. Data were analyzed using one-way analysis of variance (ANOVA) with post-hoc Tukey HSD test for multiple comparison. A pairwise comparison was conducted using Student's *t* test. Differences between groups were considered statistically significant when $P < 0.05$. Statistical analyses were performed using SPSS version 18.0 software.

2.9 Ethics Statement

The animal experiment was conducted in strict accordance with the guidelines of the Animal Welfare Act of the United States, under the protocol reviewed and approved by the Institutional

Animal Care and Use Committee of the University of Pennsylvania (IACUC#805529). The plaque-biofilm samples collection from S-ECC children were approved by Institutional Review Board (IRB) at University of Pennsylvania (IRB 824243) and were used only for the sole purpose of biofilm formation on enamel surfaces. The written permission form for each child was reviewed and signed by their legal guardians. The whole saliva is a convenient sample (with no identifiers) collected for the sole purpose of coating the hydroxyapatite discs for the in vitro biofilm studies. All adult subjects provided written informed consent (no children participated in the saliva collection) under the protocol reviewed and approved by the University of Pennsylvania Research Subject committee (IRB#818549).

CHAPTER 3: RESULTS

In this study, we developed Dex-NZM for the treatment of biofilms associated with dental caries. Since dextran is a FDA approved polymer, and dextran-coated iron oxide nanoparticles such as Feridex and Ferumoxytol, have been FDA-approved and used for magnetic resonance imaging^{36,62} and treating iron deficiency anemia⁶³, we hypothesized that the presence of a dextran coating on the nanoparticle surface could enhance biofilm targeting specificity and biocompatibility without significantly impacting the catalytic activity of the iron oxide core^{43,64,65}. We tested several different formulations that were synthesized using different dextran molecular weights and found that 10 kDa Dex-NZM provided an optimal balance of catalytic activity, biofilm uptake, and when exposed to low H₂O₂ concentration, resulted in marked bacterial killing and biofilm reduction, preventing caries severity without adverse effects *in vivo*.

3.1 Dextran-Coated NZM Maintain Catalytic Activity

Dex-NZM formulations were synthesized using a range of dextran molecular weights since we sought to understand the effect of the molecular weight of the coating on catalytic activity, biofilm incorporation, and antibiofilm effects. TEM of Dex-NZM formulations revealed that nanoparticles were formed in each case (Figure 10a). The core sizes of Dex-NZM coated with 1.5, 5, 10, 25, and 40 kDa dextran are 32.5 ± 14.2 , 14.7 ± 3 , 11.4 ± 1.8 , 15.6 ± 3.6 , and 32.2 ± 9.6 nm, respectively. The iron oxide cores formed with 5, 10, and 25 kDa dextran were similar in morphology, whereas very heterogeneous iron oxide cores were formed when 1.5 and 40 kDa dextran was used. The hydrodynamic diameters of these Dex-NZM formulations range from 30 to 60 nm, without a clear correlation with dextran molecular weight (Figure 10b). Unsurprisingly, their zeta potentials were similar, all being slightly negative, consistent with other reports for dextran-coated iron oxide nanoparticles (Figure 10b)⁶⁶. The peroxidase-like activities of Dex-NZM were measured using the

colorimetric TMB assay. These experiments were done at pH 4.5, 5.5, and 6.5 to span the range of pH values expected to exert catalytic activity. Stronger catalytic activities were observed at more acidic pH, i.e., 4.5 (found in cariogenic biofilms^{7,67}) compared to pH 6.5 (noncariogenic) for all formulations, indicating that damage caused by reduction of hydrogen peroxide and consequent generation of reactive oxygen species would be higher against pathological biofilms (Figure 10c). Interestingly, the highest catalytic activity was observed for the 10 kDa dextran formulation, which is likely due to it having the smallest core size and thus highest surface area.

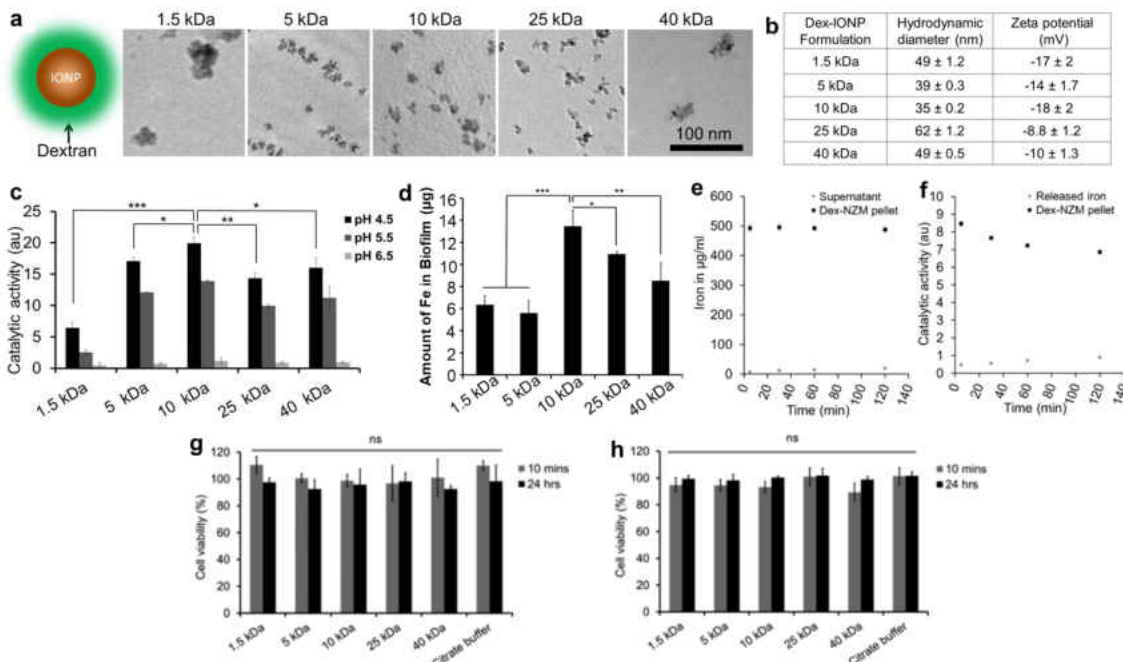


Figure 10. Characterization of Dex-NZM. (a) Schematic and TEM of Dex-NZM formulations (scale bar for all images is the same, i.e., 100 nm). (b) Hydrodynamic diameters and zeta potentials of Dex-NZM measured in DI water. (c) Catalytic activity of different Dex-NZM formulations at three different pH values, as determined from the colorimetric TMB assay. (d) Amount of Dex-NZM bound within biofilms. (e) Dex-NZM iron release assay at pH 4.5. (f) Determination of catalytic activity of released iron ions and Dex-NZM pellet. Minimal amounts of free iron ions were released at acidic pH and significantly higher catalytic activity was observed with Dex-NZM pellet compared to released iron ($P < 0.001$). (g) Effect of Dex-NZM formulations on the viability of primary human gingival epithelial cells and (h) human fibroblast cells. *, **, and *** indicate statistically significant differences of $P < 0.05$, $P < 0.01$, and $P < 0.001$, respectively. Error bars are standard deviations. "ns" stands for nonsignificant difference.

To determine whether Dex-NZM were taken up in biofilms, we performed topical treatments using an established saliva-coated hydroxyapatite (pellicle-coated tooth mimetics) biofilm model under cariogenic conditions using the oral pathogen *S. mutans* grown in the presence of sucrose (Figure 7). We found that these nanoparticles were retained within biofilms when applied topically and

that 10 kDa Dex-NZM was taken up to the greatest extent as determined by ICP-OES (Figure 10d). We also examined whether the activation of H₂O₂ by Dex-NZM is due to catalytic activity from nanoparticles themselves or from released iron ions via the Fenton reaction. We found only trace amounts of free iron ions leached from Dex-NZM in acidic pH buffer (pH 4.5, Figure 10e). Importantly, the catalytic activity of the solution phase is low (Figure 10f), showing that the observed activity is primarily derived from the nanoparticle itself. Furthermore, the biocompatibilities of Dex-NZM formulations were tested with human primary oral gingival cells and human fibroblast cells. We found that none of the Dex-NZM formulations inhibited the viability of either cell type when incubated at a concentration of 0.5 mg of iron/mL (Figure 10g,h). When selecting which formulation to pursue for further in-depth studies, i.e., analysis of catalytic activity, binding specificity, bacterial killing, EPS degradation, *ex vivo* biofilm prevention and *in vivo* testing, we chose the 10 kDa dextran formulation since it has the highest catalytic activity and biofilm uptake. Moreover, the FDA approved dextran-coated iron oxide nanoparticle uses 10 kDa dextran³⁶, further motivating more detailed study of this formulation and its use for *in vivo* efficacy evaluation.

3.2 Dextran Coating Influences on Catalytic Activity, Stability, and NZM Biofilm Binding

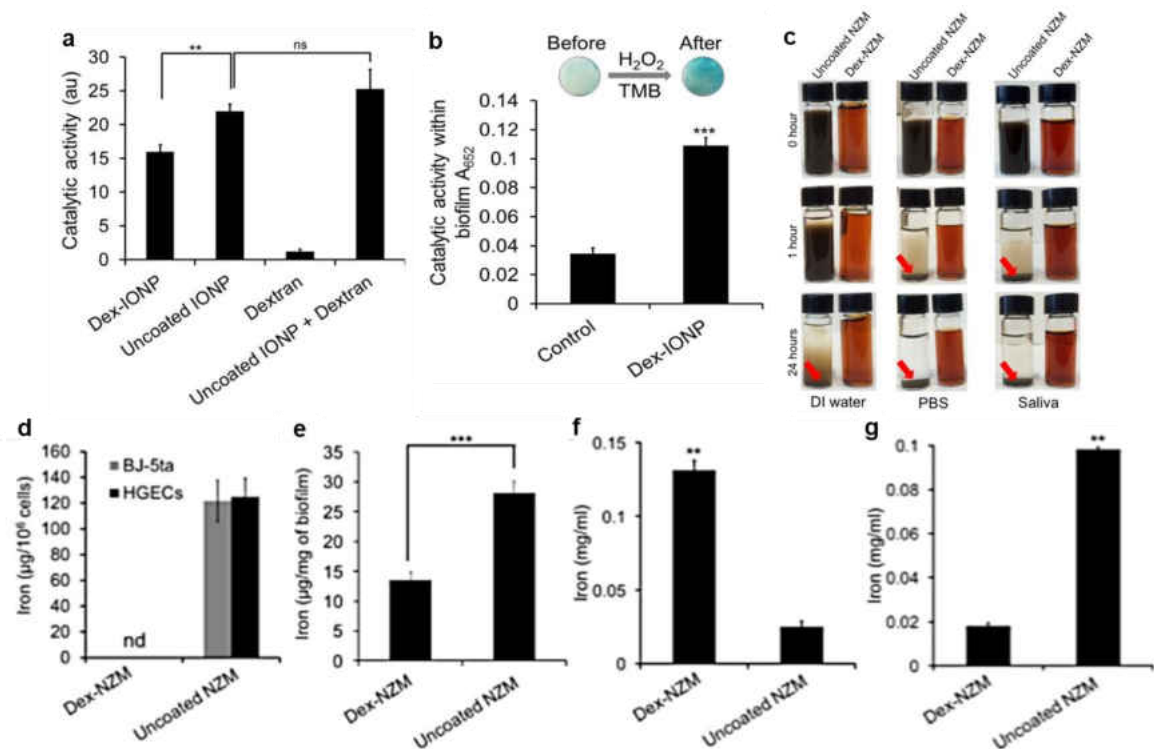
To further understand the behavior of Dex-NZM, we performed additional studies to assess catalytic performance and bioactivity in detail, including the role of dextran (vs uncoated NZM) on biofilm uptake and incorporation into biofilm structure via EPS. We compared the catalytic activity of Dex-NZM and uncoated NZM of similar core size to Dex-NZM and found that the dextran coating reduced activity somewhat, in line with results found by others⁶⁴ (Figure 11a). Furthermore, the activity of dextran alone was very low and, when dextran was mixed with uncoated NZM at the concentration found in Dex-NZM (5.4:1 dextran to iron mass ratio), there

was not a statistically significant difference in activity compared with uncoated NZM alone. Therefore, dextran coatings do not contribute to catalytic activity, but allow reagents to access iron oxide cores so that catalytic activity occurs. Furthermore, we found that Dex-NZM was catalytically active within a cariogenic biofilm (Figure 11b).

Given that dextran coating could enhance dispersibility and exogenous dextran can be incorporated into EPS matrix^{22,68}, we hypothesized that Dex-NZM could display improved formulation stability and binding specificity toward biofilms rather than mammalian tissues or uncolonized tooth surfaces. In order to probe this question, we used the aforementioned uncoated NZM as a comparator. The Dex-NZM was stable and did not settle in any of the media tested, underscoring the potential clinical utility and commercial potential of this agent (settling in storage could result in uneven dosing to the subject). We found that Dex-NZM is well suspended in water, PBS, and saliva (Figure 11c), but uncoated NZM are not stable in PBS and saliva as evidenced by settling to the bottom of the vial when suspended in PBS or saliva (at 1 h) and even in DI water (at 24 h). Next, we tested the selectivity of uncoated and dextran-coated NZM. Excitingly, we found that Dex-NZM was unable to bind to mammalian cells (both oral gingival and fibroblast cells), whereas uncoated NZM bound very strongly and in high amounts, as evidenced by ICP-OES measurements (Figure 11d). On the other hand, Dex-NZM and uncoated NZM were both taken up in biofilms significantly (Figure 11e).

We further examined the uptake of these nanoparticles in biofilms by testing their incorporation into EPS formed on hydroxyapatite surfaces via the action of GftB. Dex-NZM were incorporated into EPS to a much greater extent than uncoated NZM (Figure 11f), likely due to Dex-NZM's

chemical similarity to dextran, which can be incorporated into the EPS structure during glucan synthesis by *S. mutans*-derived GtfB exoenzymes via acceptor reaction²². Moreover, we examined the binding of these nanoparticles to saliva coated hydroxyapatite (sHA) as a tooth surface mimetic and observed that Dex-NZM had much lower binding to the apatitic surface than uncoated NZM (Figure 11g). Thus, we unexpectedly found that while Dex-NZM were taken up by biofilms, they were unable to bind to mammalian cells and less avidly to sHA, while uncoated iron oxides were bound to all tested surfaces, highlighting the selectivity of Dex-NZM toward biofilms.



3.3 In Vitro Bioactivity of Dex-NZM

The Dex-NZM activation of H_2O_2 indicated that it could, therefore, function as a bacterial killing and EPS degrading system for targeting the acidic biofilm microenvironment. To assess the

bioactivity of Dex-NZM-mediated H₂O₂ catalysis, we conducted high-resolution time-lapsed imaging using fluorescently labelled bacterial cells (*S. mutans*) and insoluble α -glucans (Figure 12). Dex-NZM (1 mg/mL) was added to an actively growing bacterial cells suspension followed by exposure to H₂O₂ at a concentration of 1%, under acidic (4.5) or near neutral pH (6.5) conditions. To visually observe the distribution of viable and dead bacteria, intact *S. mutans* cells were labelled with SYTO 60 and propidium iodide (PI) was used to determine bacterial killing over time at the single-cell level. The fluorescence images show that *S. mutans* viability was affected as early as 10 min by Dex-NZM in the presence of H₂O₂ at pH 4.5. Bacterial cells are labelled in blue by SYTO 60 and the purple color indicates dead cells labelled by PI, a cell-impermeant molecule that can only enter cells with damaged membranes, rapidly gaining intracellular access following treatment (Figure 12a). In addition, close-up views of individual bacterial cells with high magnification show Dex-NZM (labelled with Alexa Fluor 488, in yellow) located on the cell surface (Figure 12b, c).

Insoluble glucans are key virulence factors as they form the core of the extracellular matrix in cariogenic biofilms¹. Thus, we also assessed whether these EPS can be broken down following incubation with Dex-NZM and H₂O₂. The EPS were labelled by Alexa Fluor 647-dextran conjugate during glucan synthesis as detailed previously²², allowing structure visualization and degradation monitoring via time-lapse imaging. As shown in Figure 12d, the glucans (in red) were readily degraded when exposed to Dex-NZM and H₂O₂ in acidic pH. To further understand the EPS breakdown process over time, we applied computational analysis that generates geometrical scaffolds based on connectivity, topology, and length of the glucan structure. Intact glucans show a web-like structure, forming a meshwork of interwoven “EPS filaments” (Figure 12d, blue lines). However, after exposure to Dex-NZM and H₂O₂, we observed gradual dismantling of the matrix

structure by degrading the interconnected branches (see white arrowheads), resulting in a smaller EPS core with most of the shorter fragments completely degraded after 40 min (Figure 12d). These results indicate efficient bacterial killing with EPS degrading capabilities when Dex-NZM-mediated H_2O_2 catalysis is triggered at acidic pH.

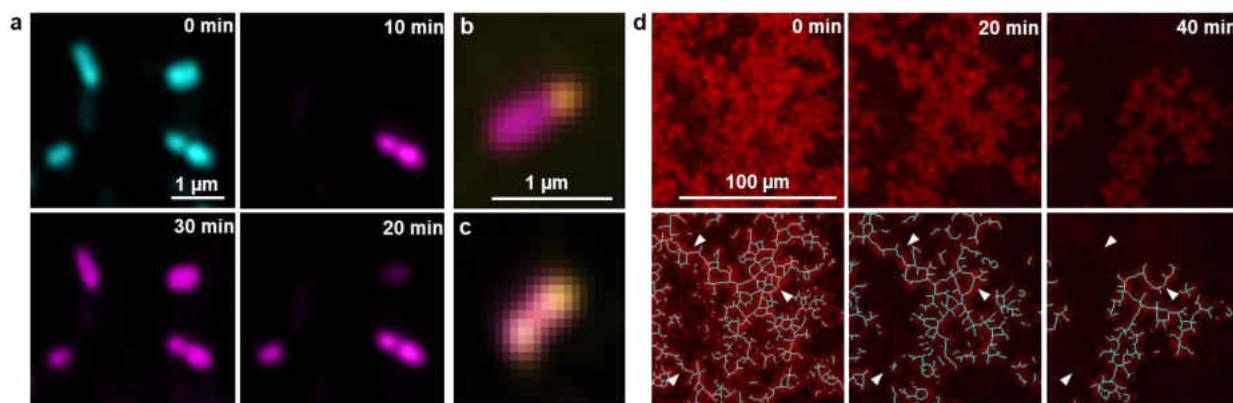


Figure 12. Time-lapsed bacterial killing and glucan degradation by Dex-NZM-activated H_2O_2 . (a) Bacterial cells are labelled in blue by SYTO 60 and dead cells in purple by propidium iodide (n=4). High-magnification close-up views of (b,c) single bacterial cell showing nanoparticles (labelled with Alexa Fluor488, in yellow; upper/lower panels) bound to its surface.(d) Time-lapsed EPS glucans (labelled in red with Alexa Fluor 647-dextranconjugate) degradation by Dex-NZM-activated H_2O_2 catalysis (n=4).

3.4. Antibiofilm Activity of Dex-NZM

To further assess the Dex-NZM binding and antibiofilm activity, we employed high-resolution confocal fluorescence imaging combined with quantitative computational analysis. Alexa-488 conjugated Dex-NZM was employed to visualize the nanoparticle distribution within biofilm architecture. Representative confocal images show Dex-NZM (labeled in green) associated with the entire bacterial cluster (in gray) and also incorporated throughout the EPS matrix (in purple) structure (Figure 13a-d). This was confirmed by energy dispersive spectroscopy (EDS), where Fe signals was found in the EDS spectra of Dex-NZM-treated biofilm (Figure 13e), additionally illustrating the successful incorporation of Dex-NZM into biofilms following topical treatment. Considering the effective Dex-NZM binding and catalytic activity within biofilms, we investigated whether the bound nanoparticles could catalyze H_2O_2 to breakdown the EPS matrix and kill the

embedded bacteria *in situ*. We found that the numbers of dead bacteria (in red) markedly increased (Figure 13g, h), and concurrently, the EPS matrix (in purple) was degraded (Figure 13i, k), indicating antibiofilm effects *in situ* via the catalytic activity of Dex-NZM. To further confirm the bioactivity of Dex-NZM, the number of viable cells and EPS content were determined in the treated biofilms. The results show potent biocidal activity against *S. mutans* within biofilm, causing > 6-log reduction of viable cells compared to vehicle control and > 1000-fold more effective than H₂O₂ alone (Figure 13l, $P < 0.01$ – 0.001 by paired *t* test). Importantly, the treatment significantly reduced the amount of insoluble glucans compared to control and to H₂O₂ or Dex-NZM alone, further indicating the EPS-degrading capability of Dex-NZM-mediated H₂O₂ catalysis (Figure 13m, $P < 0.001$ by paired *t* test).

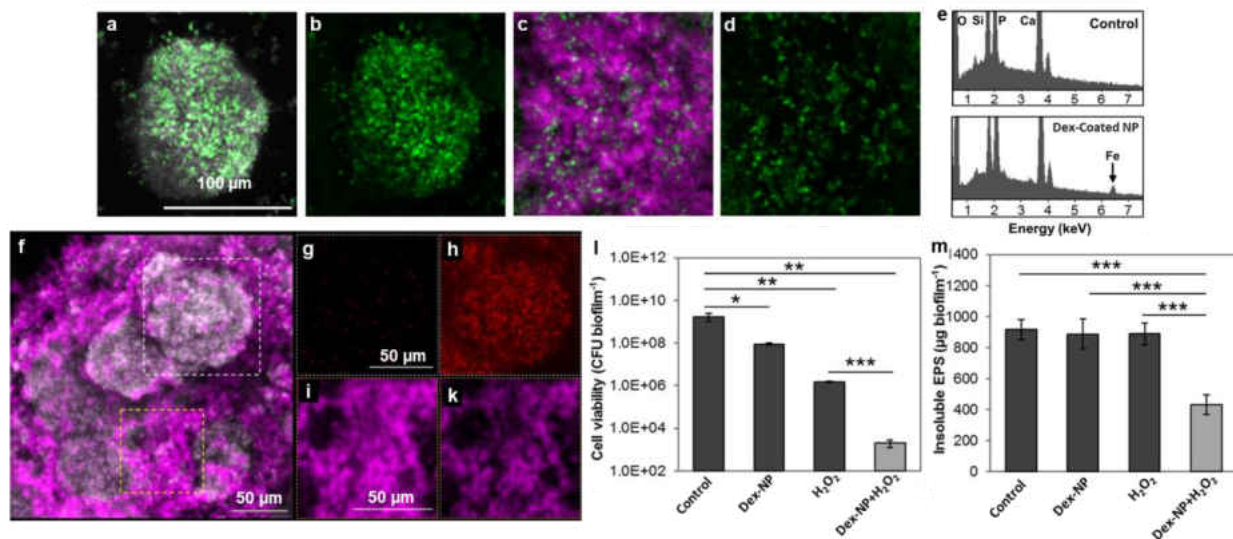


Figure 13. Antibiofilm performance of Dex-NZM/H₂O₂. (a–d) Distribution of Dex-NZM within a biofilm (gray: bacteria, green: Dex-NZM, magenta: EPS). (a) Bacterial and Dex-NZM merged image. (b) Dex-NZM image only. (c) EPS and Dex-NZM merged image. (d) Dex-NZM image only. (e) EDS spectra of untreated and Dex-NZM-treated biofilms. Representative image of a Dex-NZM treated *S. mutans* biofilm (f) before addition of H₂O₂; dashed white and yellow boxed indicate selected areas for localized antibiofilm effects of Dex-NZM. Close-up views of bacteria and EPS images before H₂O₂ exposure (panels g and h, respectively) and 100 min after H₂O₂ exposure (panels i and k). Comparison of (g) and (h) highlights the bacterial killing, while comparison of (i) and (k) indicates EPS-matrix degradation. All bacteria are displayed in gray, and the EPS-matrix is displayed in magenta in (f). Dead bacteria are displayed in red in (g) and (h). The EPS matrix is displayed in magenta in (i) and (k). (l) Effect on the viability of *S. mutans* cells within biofilms as well as EPS degradation (m) following exposure to Dex-NZM and/or H₂O₂. * $P < 0.05$, ** $P < 0.01$, *** $P < 0.001$.

3.5 Disruption of *Ex Vivo* Biofilms and Human Enamel Demineralization

We next developed a combination therapy consisting of topical application of Dex-NZM (at 1 mg/mL) immediately followed by H₂O₂ (at 1%) exposure, twice daily to simulate oral use. To gain

further insight into the therapeutic potential of our approach, we used an *ex vivo* human biofilm model to assess whether Dex-NZM/H₂O₂ can disrupt cariogenic biofilm and prevent enamel surface damage. In this model, plaque-biofilm samples were collected from diseased patients affected by severe childhood caries and inoculated for biofilm development on natural human tooth-enamel (Figure 8). The microscale spatial distribution and structural organization of the biofilm components were determined via a multi-labeling approach using total bacteria and *S. mutans* specific fluorescent probes, with EPS-matrix labeling via an Alexa Fluor 647-dextran conjugate. The control human-derived biofilms had ‘dome-shaped’ bacterial clusters (in blue) spatially arranged with EPS (in red) matrix (Figure 14a) that are typically found when grown under cariogenic conditions in the presence of sucrose. Cross-sectional confocal images reveal localized bacterial aggregates comprised mostly of *S. mutans* cells (in green, Figure 14a bacteria panel) that are surrounded by an interconnected EPS-matrix (in red, Figure 14a EPS panel) forming cohesive and densely packed microbial structure. In a sharp contrast, only small cell clusters with sparsely distributed EPS were detected in the Dex-NZM/H₂O₂ treatment group (Figure 14b).

The striking differences in both bacterial density and structural organization could inflict differential damage of the mineralized tooth tissue underneath the distinctive biofilms. Macroscopically, we observed large areas of enamel surface demineralization in the control group; close-up views show chalky and white spot-like demineralization, similar to early caries lesions seen clinically (Figure 14c). In contrast, the enamel surface from Dex-NZM/H₂O₂ treatment was essentially devoid of such opaque demineralized areas (Figure 14e). The observed visual differences were confirmed with confocal topography imaging and transversal microradiography analysis. The enamel surfaces from the control group have eroded forming microcavities resulting in ~10 times higher surface roughness (*Sa* values) than that treated with Dex-NZM/H₂O₂, whose

enamel surface was mostly intact and smooth (Figure 14g, h). Importantly, the lesion depth as determined by microradiography is significantly deeper in the control group (vs. Dex-NZM/H₂O₂ group, Figure 14d, f, $P < 0.01$ by paired t test).

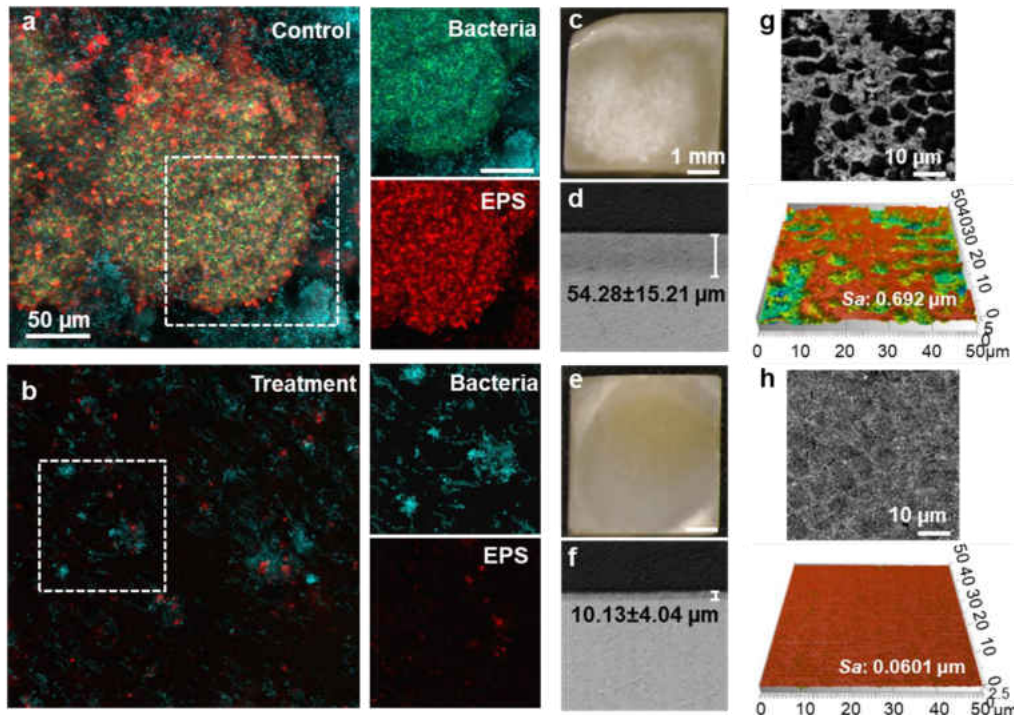


Figure 14. Antibiofilm properties of topical Dex-NZM/H₂O₂ treatments using an *ex vivo* biofilm model. (a, b) Confocal imaging of the morphology of vehicle-control treated biofilm and biofilm treated with Dex-NZM/H₂O₂ (white box indicates selected area for close-up images of bacteria and EPS components): total bacteria and *S. mutans* cells are labelled in blue and green, respectively; EPS are in red. (c, e) Light microscopy images of the enamel surface of untreated biofilm showing “white spot-like caries lesions” and Dex-NZM/H₂O₂ treated biofilm showing intact and smooth surface. (d, f) Lesion depth of the enamel surfaces (control and treated). (g, h) Representative confocal topography of enamel surfaces and enamel roughness (control and treated).

Altogether, the *in vitro* data demonstrate biofilm targeting specificity by Dex-NZM, which in turn can effectively kill bacterial cells and degrade EPS matrix in pathogenic acidic biofilms when activated by H₂O₂. The Dex-NZM-mediated H₂O₂ catalysis can potentially disrupt the development of cariogenic biofilms and prevent localized demineralization and caries-like lesions on tooth-enamel surface. These results indicated that Dex-NZM, when used as a topical oral treatment, would be selective for biofilms over the host tissues in the oral cavity, impacting caries development while sparing mammalian host cells *in vivo*.

3.6 *In Vivo* Inhibition of Dental Caries

The *in vivo* efficacy of Dex-NZM as an anti-caries treatment was evaluated in a well-established rodent model of dental caries⁵². In addition to mineralized tooth tissue, both the effects on soft tissue and on the oral microbiota composition/diversity were examined. In this model, tooth enamel progressively develops caries lesions (analogous to those observed in humans), proceeding from initial areas of demineralization to moderate lesions and on to extensive (severe) lesions characterized by enamel structure damage and cavitation. We simulated the treatment conditions that might be experienced clinically in humans by applying the test agent solutions topically twice daily with a brief, 1 min exposure time. We found that Dex-NZM/H₂O₂ treatment was highly effective in reducing caries development in both smooth and sulcal surfaces (Figure 15a, b), resulting in significantly less overall caries lesions compared to vehicle control and Dex-NZM or H₂O₂ alone. Importantly, the severity of caries lesions was progressively blocked and completely prevented extensive lesions and cavitation on smooth dental surface. Furthermore, the efficacy of Dex-NZM/H₂O₂ was significantly higher than H₂O₂ or Dex-NZM alone (Figure 15a, b), supporting the catalytic-therapeutic mechanism of Dex-NZM activation of H₂O₂ via its intrinsic catalytic activity.

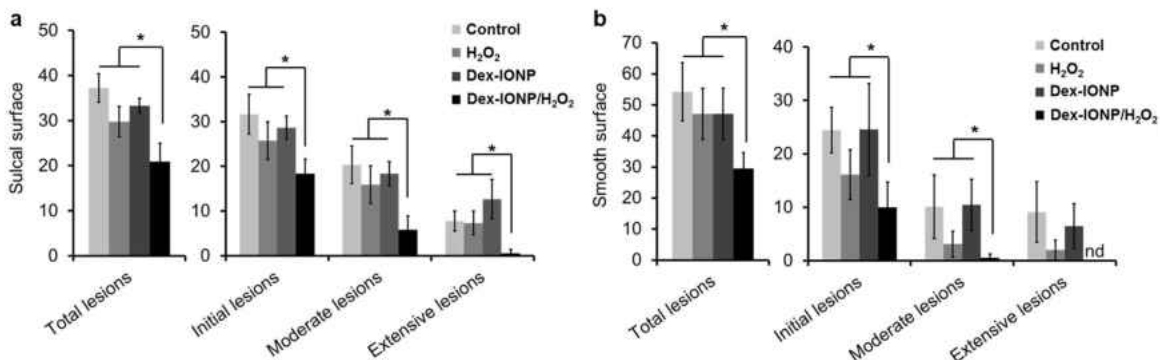


Figure 15. Effect of Dex-NZM/H₂O₂ on dental caries *in vivo*. (a) Caries scores recorded from sulcal surface. (b) Caries scores recorded from smooth surface. The caries scores were recorded according to Larson's modification of Keyes' scoring system, and the data are presented as mean ± SD (n = 10). * indicates significant differences (P < 0.05) from control, H₂O₂, or Dex-NZM.

In vivo data provided further validation of biocompatibility after 21 days of topical treatment via analysis conducted on the gingival tissues and the oral microbiota. Histopathological analysis on gingival and palatal tissues revealed no visible signs of adverse effects, such as proliferative changes, inflammatory responses, or necrosis, of treatment with Dex-NZM, or H₂O₂ or the Dex-NZM/H₂O₂ (Figure 16a). This result supports our *in vitro* findings showing that Dex-NZM lacks cytotoxic effects and more selectively binds to bacterial biofilms rather than gingival epithelial cells. The effects of Dex-NZM/H₂O₂ on oral microbiota were also evaluated, and no statistically significant changes of oral microbial composition and diversity were found between the treatment groups (Figure 16b, c). Taken together, the data show that topical Dex-NZM/H₂O₂ treatments can efficiently suppress the development of a costly and prevalent oral disease without affecting the oral microbiota composition or showing deleterious effects in the surrounding soft tissues *in vivo*.

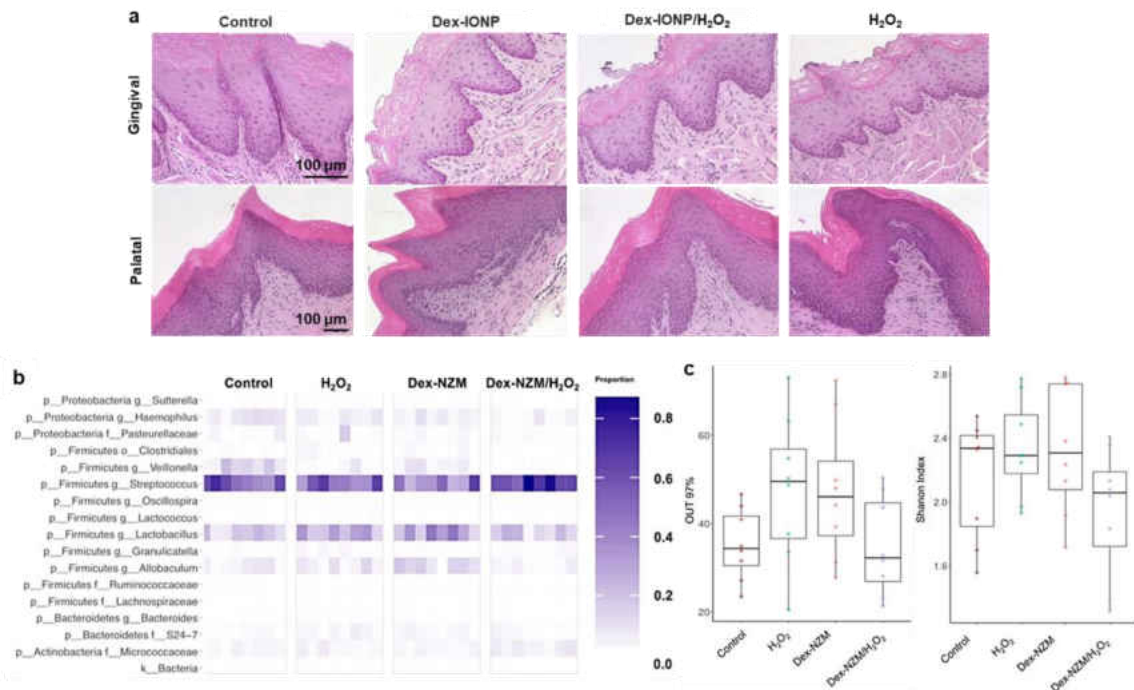


Figure 16. Effects of topical Dex-NZM/H₂O₂ on oral microbiome and soft tissue *in vivo* after 21 days of treatment. (a) Histopathology of gingival and palatal tissue in animals treated with Dex-NZM/H₂O₂ is similar to control. (b) The heatmap shows main bacterial genera found across all samples, distributed by treatment groups. (c) Richness and diversity show no significant differences among groups ($P > 0.05$ by Wilcoxon rank sum test).

CHAPTER 4: DISCUSSION

We report herein that dextran-coated iron oxide nanozymes are an effective antibiofilm agent that can be used for treatment of a ubiquitous oral disease, dental caries. The observation of catalytic activity arising from coated iron oxide nanoparticles is important. Surface coating of nanozymes can affect their enzyme-like activity, since binding of the coating to the nanoparticle reduces the surface available to interact with substrates^{64,69}. In biological applications of nanozymes, it is often necessary to find coatings that provide both stability in physiological fluids as well as allow access of substrates to the nanoparticle surface⁷⁰.

We found that dextran coating did not silence the peroxidase-like activity of iron oxide nanoparticles. This finding agrees with a previous report⁶⁴, although the iron oxide nanoparticles were more than 10-fold larger than in this study. It also agrees with previous reports of dextran coating of iron oxide nanoparticles leaving gaps on their surfaces⁷¹. This property may play a role in other bioactivities that have been observed to arise from iron oxide nanoparticles^{72,73}. It may be the case that this catalytic activity could be used against biofilms in other settings such as joint replacements or catheters. The efficacy of the Dex-NZM/H₂O₂ combination may indicate that other peroxidase mimics, such as graphene⁴⁰, will have similar antibiofilm effects. In addition, the biofilm targeting effect that we found with dextran could potentially be used with other materials such as gold nanoparticles⁷⁴. The advantages of Dex-NZM are further highlighted by their comparison with uncoated NZM. We found that uncoated NZM bind indiscriminately to biofilms and tissues in the mouth (i.e., they bound to mammalian cells and hydroxyapatite), whereas Dex-NZM bound more selectively to biofilms. Moreover, we found that Dex-NZM were well suspended in different solutions tested, while the uncoated NZM settled rapidly in each fluid. The settling of a formulation is a significant drawback for practical consumer product development

since the dose might be dispensed unevenly, leading to reduced effectiveness in addition to possible adverse effects due to unspecific binding.

Dex-NZM display peroxidase-like activity at pathological acidic pH values found in cariogenic biofilms but attenuated at pH values close to neutral (physiological), avoiding unmitigated free radical production. Dex-NZM retained within biofilms can locally activate H₂O₂ for *in situ* bacterial killing via membrane disruption and EPS matrix degradation through glucan structure cleavage. Such properties thwarted cariogenic biofilm accumulation and prevented enamel surface damage, suppressing the onset of severe caries lesions, without deleterious side effects *in vivo*. This therapeutic approach may have broader reach as EPS are important components of matrices in most biofilms² and acidic pH microenvironments can be found in other pathological conditions, such as in cystic fibrosis and *Staphylococcal* infections^{75,76}. Thus, exploitation of catalytic actions by clinically approved nanomaterials could open up a new avenue for prevention of infectious diseases.

Current antimicrobial approaches, including silver nanoparticles, chlorhexidine, hydrogen peroxide, and other chemical biocides are incapable of degrading EPS and ineffective against dental caries^{28,77}. Fluoride, introduced over 60 years ago, as well as more recent nanoapatites can reduce demineralization and promote remineralization but has limited antibiofilm effects²⁸. We have thus discovered a topical use of Dex-NZM to expand the few clinically available options for caries-preventive therapy. Immediate clinical applications of Dex-NZM-mediated catalysis could entail potentiating the efficacy of existing peroxide-based modalities, including mouthrinses and toothpastes, which contain 1.5-10% H₂O₂. Dex-NZM could be locally delivered using containers with separate chambers that can keep the iron oxide nanoparticles and H₂O₂ separated in storage, but allowing mixing at the time of product delivery (rinsing or brushing). In terms of dosage, the

rodent caries model has contributed to the development of clinically effective toothpastes and related caries-preventive products, including assessment of optimal fluoride concentration {REF?}. Thus, the currently tested topical dosage may achieve therapeutic effects clinically, although further optimization of Dex-NZM and H₂O₂ concentrations may be required to develop a cost effective, safe and efficacious treatment.

Dex-NZM might have applications for other oral diseases and against additional bacterial strains⁷⁸; however, this technology may have limitations when the local pH environment is not acidic (e.g., periodontal diseases) or with microorganisms that can degrade H₂O₂. Another potential drawback is the possibility of iron staining of enamel. We found that Dex-NZM to bound poorly to saliva-coated hydroxyapatite *in vitro* and minimally leached free irons even at acidic pH, and we did not observe any discoloration over the 21-day period of the *in vivo* experiment. Nevertheless, more extensive testing will be required to establish that Dex-NZM does not stain teeth in humans. Lastly, lack of visualization of biofilms on the teeth from the animal experiments and unavailability of appropriate uncoated NZM control due to its aforementioned issues are experimental limitations of this study. Further detailed analysis of the *in vivo* biofilms following treatment and inclusion of NZM control with inert non-dextran coatings in addition to dosage and treatment duration optimization shall reveal important mechanistic insights as well as advance this catalytic nanotherapeutic approach.

The iron-oxide-particle-based system has many inherent advantages over other nanoparticle-based systems. It is a drugfree approach, thus overcoming limitations of drug dosing, requirement of drug loading compatibilities, and risks associated with drug resistance. However, there are still outstanding questions regarding the clinical translation of the approach, including potential off-target effects within the oral cavity and systemically for the Dex-NZM system and other

nanoparticle approaches. Nonspecific off-target effects of oral anti-biofilm treatments can occur both immediately to local tissues and after clearance of nanoparticles. The predominant clearance route of topical treatments in the mouth is via ingestion, which may result in systemic circulation and tissue distribution. Therefore, it is critical to evaluate potential off-target biodistribution and effects prior to translation into new antibiofilm nanotechnologies. This point is especially true for oral biofilm therapies. Human caries affects all ages, and treatment is a persistent challenge. Thus, chronic off-target accumulation of nanoparticles may result in long-lasting effects. Metal or metal-oxide-based nanoparticles can be absorbed within the gastrointestinal tract. Although bioavailability may be low (e.g., <5% of ingested dose), off-target systemic effects of nanoparticles have been reported³³. Metal nanoparticles with larger doses have resulted in weight loss and increases in oxidative stress in blood, liver, brain, kidney, and spleen⁷⁹, with long-term residence in the brain⁸⁰. In addition, tissue fibrosis^{81,82} and DNA damage have been reported⁸³. Although it is unclear if iron oxide particles will have similar toxicity profiles, their likely transport through the acidic stomach milieu, which will itself result in robust radical production, motivates careful evaluation of systemic effects of this powerful oral biofilm treatment strategy as well as other nanoparticle-based approaches.

In summary, Dex-NZM is very stable in saliva or physiological buffers, does not bind to mammalian cells, is retained within bacterial biofilms, and is effective in reducing dental caries without deleterious effects on the surrounding soft oral tissues. In addition, Dex-NZM/H₂O₂ does not adversely affect oral microbiota diversity and composition. The translation of this treatment to use in humans is likely practical, since the costs of the various reagents, such as iron salts and hydrogen peroxide, are quite low and readily available. The treatment could be supplied as a mouthwash with a bottle containing two chambers or in toothpaste form where the nanoparticles

and hydrogen peroxide are kept separate until the toothpaste is dispensed. It might be possible to develop a formulation that self-generates hydrogen peroxide, thereby circumventing the need for two chambers in the container, although such an agent may be more complex and expensive. Additional dosing and safety studies would have to be done before testing in humans; however, the prior FDA-approval of similar iron oxide nanoparticles for systemic use (at several hundred-fold higher dosage) and the limited exposure received via topical applications in the oral cavity provide reasons to be optimistic about the safety of this approach. We also envision this therapeutic approach to be particularly useful for patients with or at high risk of developing severe childhood caries, an aggressive form of disease characterized by rampant tooth decay, that is often associated with iron deficiency.

CONCLUSIONS

Dextran-coated iron oxide nanozymes are an effective antibiofilm agent for an oral disease. Despite the dextran coating, these nanozymes possess peroxidase-like catalytic activity and have additional attractive attributes such as stability and targeting specificity. Dex-NZM display peroxidase-like activity at pathological acidic pH values, efficiently target biofilm cells, and degrade EPS matrix via catalytic activation of H₂O₂. Further analyses revealed that the catalytic activity arises from the iron cores of these nanoparticles and that their dextran coating provides selective binding to bacterial cells over oral epithelial cells while facilitating incorporation into biofilm matrix (Figure 17). *In vivo* results showed that Dex-NZM mediated H₂O₂ catalysis potently disrupted the onset of a costly and highly prevalent oral biofilm-associated infection (dental caries or tooth decay). The nanozyme-based topical therapy markedly reduced the number and severity of caries lesions compared to controls. Histological and microbiome analyses revealed no adverse effects on the surrounding host tissues and oral microbiota diversity *in vivo*, consistent with lack

of cytotoxicity and biofilm-targeting specificity observed *in vitro*. Altogether, Dex-NZM is a potent and biocompatible antibiofilm agent. There are limitations of this technology, such as when the local pH environment is not acidic or against bacterial strains that can degrade H_2O_2 , while the potential of tooth staining and in-depth safety studies need to be conducted and assessed. Nevertheless, given the prior FDA-approval of similar agents, this nanozyme-based approach could provide an excellent therapeutic platform for alternative product development to prevent the burdensome of dental caries. At the same time, the availability and low cost of the materials and chemical flexibility of iron oxide nanoparticles could galvanize a wider investigation of this approach for clinical applications to treat other biofilm-related maladies.

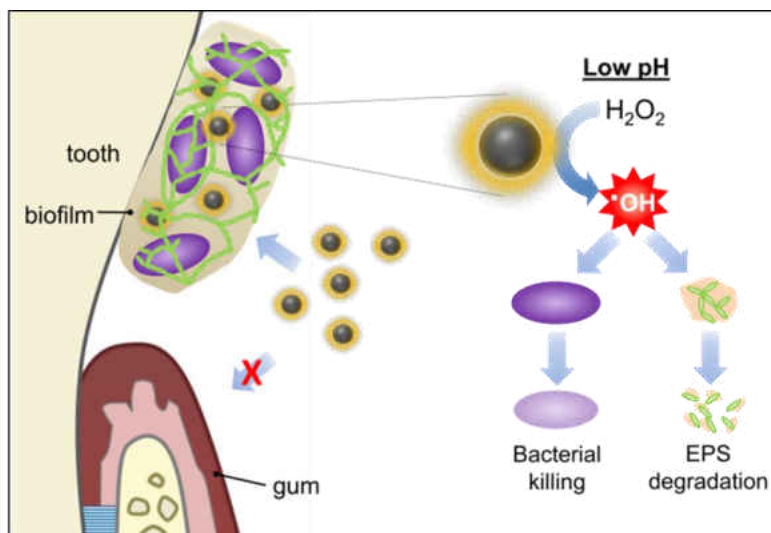


Figure 17. Schematics of biofilm disruption under acidic condition by catalytic Dex-NZM activation of hydrogen peroxide. Dex-NZM displays strong catalytic (peroxidase-like) activity at acidic pH values, target biofilms with high specificity, and activated H_2O_2 for localized bacterial killing and EPS-matrix breakdown.

REFERENCES

1. Bowen WH, Burne RA, Wu H, Koo H. Oral biofilms: Pathogens, matrix, and polymicrobial interactions in microenvironments. *Trends Microbiol.* 2018;26(3):229-242.
2. Flemming H, Wingender J, Szewzyk U, Steinberg P, Rice SA, Kjelleberg S. Biofilms: An emergent form of bacterial life. *Nat Rev Microbiol.* 2016;14(9):563.
3. Lebeaux D, Ghigo JM, Beloin C. Biofilm-related infections: Bridging the gap between clinical management and fundamental aspects of recalcitrance toward antibiotics. *Microbiol Mol Biol Rev.* 2014;78(3):510-543.
4. Marsh P, Zaura E. Dental biofilm: Ecological interactions in health and disease. *J Clin Periodontol.* 2017;44:S12-S22.
5. Maslowski KM, Mackay CR. Diet, gut microbiota and immune responses. *Nat Immunol.* 2010;12(1):5-9.
6. David LA, Maurice CF, Carmody RN, et al. Diet rapidly and reproducibly alters the human gut microbiome. *Nature.* 2014;505(7484):559-563.
7. Lamont RJ, Koo H, Hajishengallis G. The oral microbiota: dynamic communities and host interactions. *Nat Rev Microbiol.* 2018;16(12):745-759.
8. Hobley L, Harkins C, MacPhee CE, Stanley-Wall NR. Giving structure to the biofilm matrix: An overview of individual strategies and emerging common themes. *FEMS Microbiol Rev.* 2015;39(5):649-669.
9. Koo H, Falsetta M, Klein M. The exopolysaccharide matrix: A virulence determinant of cariogenic biofilm. *J Dent Res.* 2013;92(12):1065-1073.
10. Takahashi N, Nyvad B. The role of bacteria in the caries process: Ecological perspectives. *J Dent Res.* 2011;90(3):294-303.

11. Liu Y, Ren Z, Hwang G, Koo H. Therapeutic strategies targeting cariogenic biofilm microenvironment. *Adv Dent Res*. 2018;29(1):86-92.
12. Liu Y, Nascimento M, Burne RA. Progress toward understanding the contribution of alkali generation in dental biofilms to inhibition of dental caries. *Int J Oral Sci*. 2012;4(3):135-140.
13. Merritt J, Qi F. The mutacins of *Streptococcus mutans*: regulation and ecology. *Mol Oral Microbiol*. 2012;27(2):57-69.
14. Hajishengallis E, Parsaei Y, Klein MI, Koo H. Advances in the microbial etiology and pathogenesis of early childhood caries. *Mol Oral Microbiol*. 2017;32(1):24-34.
15. Bowen WH, Koo H. Biology of *Streptococcus mutans*-derived glucosyltransferases: role in extracellular matrix formation of cariogenic biofilms. *Caries Res*. 2011;45(1):69-86.
16. Leme AP, Koo H, Bellato C, Bedi G, Cury J. The role of sucrose in cariogenic dental biofilm formation—new insight. *J Dent Res*. 2006;85(10):878-887.
17. Koo H, Yamada KM. Dynamic cell–matrix interactions modulate microbial biofilm and tissue 3D microenvironments. *Curr Opin Cell Biol*. 2016;42:102-112.
18. Flemming H, Wingender J. The biofilm matrix. *Nat Rev Microbiol*. 2010;8(9):623-633.
19. Peterson BW, He Y, Ren Y, et al. Viscoelasticity of biofilms and their recalcitrance to mechanical and chemical challenges. *FEMS Microbiol Rev*. 2015;39(2):234-245.
20. Hwang G, Klein MI, Koo H. Analysis of the mechanical stability and surface detachment of mature *Streptococcus mutans* biofilms by applying a range of external shear forces. *Biofouling*. 2014;30(9):1079-1091.
21. Liu Y, Kamesh AC, Xiao Y, et al. Topical delivery of low-cost protein drug candidates made in chloroplasts for biofilm disruption and uptake by oral epithelial cells. *Biomaterials*. 2016;105:156-166.

22. Xiao J, Klein MI, Falsetta ML, et al. The exopolysaccharide matrix modulates the interaction between 3D architecture and virulence of a mixed-species oral biofilm. *PLoS Pathog.* 2012;8(4):e1002623.
23. Hwang G, Liu Y, Kim D, et al. Simultaneous spatiotemporal mapping of in situ pH and bacterial activity within an intact 3D microcolony structure. *Sci Rep.* 2016;6:32841.
24. Guo L, McLean JS, Lux R, He X, Shi W. The well-coordinated linkage between acidogenicity and aciduricity via insoluble glucans on the surface of *Streptococcus mutans*. *Sci Rep.* 2015;5:18015.
25. Autio-Gold J. The role of chlorhexidine in caries prevention. *Oper Dent.* 2008;33(6):710-716.
26. Marsh P. Contemporary perspective on plaque control. *Br Dent J.* 2012;212(12):601-606.
27. O Mullane D, Baez R, Jones S, et al. Fluoride and oral health. *Community Dent Health.* 2016;33(2):69-99.
28. Featherstone J, Doméjean S. The role of remineralizing and anticaries agents in caries management. *Adv Dent Res.* 2012;24(2):28-31.
29. Marquis RE, Clock SA, Mota-Meira M. Fluoride and organic weak acids as modulators of microbial physiology. *FEMS Microbiol Rev.* 2003;26(5):493-510.
30. Pleszczyńska M, Wiater A, Janczarek M, Szczodrak J. (1→3)- α -d-glucan hydrolases in dental biofilm prevention and control: A review. *Int J Biol Macromol.* 2015;79:761-778.
31. Jeon JG, Rosalen PL, Falsetta ML, Koo H. Natural products in caries research: Current (limited) knowledge, challenges and future perspective. *Caries Res.* 2011;45(3):243-263.
32. Allaker RP, Memarzadeh K. Nanoparticles and the control of oral infections. *Int J Antimicrob Agents.* 2014;43(2):95-104.

33. Besinis A, De Peralta T, Tredwin CJ, Handy RD. Review of nanomaterials in dentistry: Interactions with the oral microenvironment, clinical applications, hazards, and benefits. *ACS Nano*. 2015;9(3):2255-2289.
34. Paula A, Koo H. Nanosized building blocks for customizing novel antibiofilm approaches. *J Dent Res*. 2017;96(2):128-136.
35. Horev B, Klein MI, Hwang G, et al. pH-activated nanoparticles for controlled topical delivery of farnesol to disrupt oral biofilm virulence. *ACS Nano*. 2015;9(3):2390-2404.
36. Corot C, Robert P, Idée J, Port M. Recent advances in iron oxide nanocrystal technology for medical imaging. *Adv Drug Deliv Rev*. 2006;58(14):1471-1504.
37. Gao L, Liu Y, Kim D, et al. Nanocatalysts promote *Streptococcus mutans* biofilm matrix degradation and enhance bacterial killing to suppress dental caries in vivo. *Biomaterials*. 2016;101:272-284.
38. Cormode DP, Sanchez-Gaytan BL, Mieszawska AJ, Fayad ZA, Mulder WJ. Inorganic nanocrystals as contrast agents in MRI: Synthesis, coating and introduction of multifunctionality. *NMR Biomed*. 2013;26(7):766-780.
39. van Schooneveld MM, Vucic E, Koole R, et al. Improved biocompatibility and pharmacokinetics of silica nanoparticles by means of a lipid coating: a multimodality investigation. *Nano Lett*. 2008;8(8):2517-2525.
40. Naha PC, Al Zaki A, Hecht E, et al. Dextran coated bismuth–iron oxide nanohybrid contrast agents for computed tomography and magnetic resonance imaging. *J Mater Chem B*. 2014;2(46):8239-8248.
41. Naha PC, Liu Y, Hwang G, et al. Dextran-coated iron oxide nanoparticles as biomimetic catalysts for localized and pH-activated biofilm disruption. *ACS Nano*. 2019;13(5):4960-4971.
42. Hauser AK, Mitov MI, Daley EF, McGarry RC, Anderson KW, Hilt JZ. Targeted iron oxide nanoparticles for the enhancement of radiation therapy. *Biomaterials*. 2016;105:127-135.

43. Zhang J, Zhuang J, Gao L, et al. Decomposing phenol by the hidden talent of ferromagnetic nanoparticles. *Chemosphere*. 2008;73(9):1524-1528.
44. Garg B, Bisht T, Ling Y. Graphene-based nanomaterials as efficient peroxidase mimetic catalysts for biosensing applications: an overview. *Molecules*. 2015;20(8):14155-14190.
45. Hwang G, Koltisko B, Jin X, Koo H. Nonleachable imidazolium-incorporated composite for disruption of bacterial clustering, exopolysaccharide-matrix assembly, and enhanced biofilm removal. *ACS Appl Mater Interfaces*. 2017;9(44):38270-38280.
46. Falsetta ML, Klein MI, Colonne PM, et al. Symbiotic relationship between *Streptococcus mutans* and *Candida albicans* synergizes virulence of plaque biofilms *in vivo*. *Infect Immun*. 2014;82(5):1968-1981.
47. Xiao J, Moon Y, Li L, et al. *Candida albicans* carriage in children with severe early childhood caries (S-ECC) and maternal relatedness. *PLoS One*. 2016;11(10):e0164242.
48. Liu Y, Naha PC, Hwang G, et al. Topical ferumoxytol nanoparticles disrupt biofilms and prevent tooth decay *in vivo* via intrinsic catalytic activity. *Nat Commun*. 2018;9(1):2920.
49. Xiao J, Hara AT, Kim D, Zero DT, Koo H, Hwang G. Biofilm three-dimensional architecture influences *in situ* pH distribution pattern on the human enamel surface. *Int J Oral Sci*. 2017;9(2):74-79.
50. Thurnheer T, Gmür R, Guggenheim B. Multiplex FISH analysis of a six-species bacterial biofilm. *J Microbiol Methods*. 2004;56(1):37-47.
51. Kim D, Sitepu IR, Hashidoko Y. Induction of biofilm formation in the betaproteobacterium *Burkholderia unamae* CK43B exposed to exogenous indole and gallic acid. *Appl Environ Microbiol*. 2013;79(16):4845-4852.
52. Bowen WH. Rodent model in caries research. *Odontology*. 2013;101(1):9-14.

53. Klein MI, Scott-Anne KM, Gregoire S, Rosalen PL, Koo H. Molecular approaches for viable bacterial population and transcriptional analyses in a rodent model of dental caries. *Mol Oral Microbiol.* 2012;27(5):350-361.
54. Caporaso JG, Lauber CL, Walters WA, et al. Ultra-high-throughput microbial community analysis on the illumina HiSeq and MiSeq platforms. *ISME J.* 2012;6(8):1621-1624.
55. Edgar RC. Search and clustering orders of magnitude faster than BLAST. *Bioinformatics.* 2010;26(19):2460-2461.
56. McDonald D, Price MN, Goodrich J, et al. An improved greengenes taxonomy with explicit ranks for ecological and evolutionary analyses of bacteria and archaea. *ISME J.* 2012;6(3):610-618.
57. Oksanen J, Kindt R, Legendre P, et al. The vegan package. *Community ecology package.* 2007;10:631-637.
58. Lozupone C, Knight R. UniFrac: a new phylogenetic method for comparing microbial communities. *Appl Environ Microbiol.* 2005;71(12):8228-8235.
59. Paradis E, Claude J, Strimmer K. APE: analyses of phylogenetics and evolution in R language. *Bioinformatics.* 2004;20(2):289-290.
60. Naha PC, Chhour P, Cormode DP. Systematic in vitro toxicological screening of gold nanoparticles designed for nanomedicine applications. *Toxicol In Vitro.* 2015;29(7):1445-1453.
61. Guggenheim B, Gmür R, Galicia JC, et al. *In vitro* modeling of host-parasite interactions: the 'subgingival' biofilm challenge of primary human epithelial cells. *BMC Microbiol.* 2009;9(1):280.
62. Tassa C, Shaw SY, Weissleder R. Dextran-coated iron oxide nanoparticles: a versatile platform for targeted molecular imaging, molecular diagnostics, and therapy. *Acc Chem Res.* 2011;44(10):842-852.

63. Spinowitz BS, Kausz AT, Baptista J, et al. Ferumoxytol for treating iron deficiency anemia in CKD. *J Am Soc Nephrol*. 2008;19(8):1599-1605.
64. Gao L, Zhuang J, Nie L, et al. Intrinsic peroxidase-like activity of ferromagnetic nanoparticles. *Nat Nanotechnol*. 2007;2(9):577-583.
65. Zhang L, Zhai Y, Gao N, Wen D, Dong S. Sensing H₂O₂ with layer-by-layer assembled Fe₃O₄-PDDA nanocomposite film. *Electrochemistry Communications*. 2008;10(10):1524-1526.
66. Unterweger H, Janko C, Schwarz M, et al. Non-immunogenic dextran-coated superparamagnetic iron oxide nanoparticles: a biocompatible, size-tunable contrast agent for magnetic resonance imaging. *Int J Nanomedicine*. 2017;12:5223-5238.
67. Koo H, Xiao J, Klein MI, Jeon JG. Exopolysaccharides produced by *Streptococcus mutans* glucosyltransferases modulate the establishment of microcolonies within multispecies biofilms. *J Bacteriol*. 2010;192(12):3024-3032.
68. Klein MI, Duarte S, Xiao J, Mitra S, Foster TH, Koo H. Structural and molecular basis of the role of starch and sucrose in *Streptococcus mutans* biofilm development. *Appl Environ Microbiol*. 2009;75(3):837-841.
69. Wei H, Wang E. Nanomaterials with enzyme-like characteristics (nanozymes): Next-generation artificial enzymes. *Chem Soc Rev*. 2013;42(14):6060-6093.
70. Cormode DP, Gao L, Koo H. Emerging biomedical applications of enzyme-like catalytic nanomaterials. *Trends Biotechnol*. 2018;36(1):15-29.
71. Jung CW, Jacobs P. Physical and chemical properties of superparamagnetic iron oxide MR contrast agents: Ferumoxides, ferumoxtran, ferumoxsil. *Magn Reson Imaging*. 1995;13(5):661-674.
72. van Tilborg GA, Cormode DP, Jarzyna PA, et al. Nanoclusters of iron oxide: Effect of core composition on structure, biocompatibility, and cell labeling efficacy. *Bioconjug Chem*. 2012;23(5):941-950.

73. Vasanawala SS, Nguyen K, Hope MD, et al. Safety and technique of ferumoxytol administration for MRI. *Magn Reson Med*. 2016;75(5):2107-2111.
74. Chiu RY, Nguyen PT, Wang J, Jue E, Wu BM, Kamei DT. Dextran-coated gold nanoprobe for the concentration and detection of protein biomarkers. *Ann Biomed Eng*. 2014;42(11):2322-2332.
75. Mercier R, Stumpo C, Rybak MJ. Effect of growth phase and pH on the *in vitro* activity of a new glycopeptide, oritavancin (LY333328), against *Staphylococcus aureus* and *Enterococcus faecium*. *J Antimicrob Chemother*. 2002;50(1):19-24.
76. Poschet J, Perrett E, Deretic V. Hyperacidification in cystic fibrosis: links with lung disease and new prospects for treatment. *Trends Mol Med*. 2002;8(11):512-519.
77. Koo H, Allan RN, Howlin RP, Stoodley P, Hall-Stoodley L. Targeting microbial biofilms: current and prospective therapeutic strategies. *Nat Rev Microbiol*. 2017;15(12):740-755.
78. Bukhari S, Kim D, Liu Y, Karabucak B, Koo H. Novel endodontic disinfection approach using catalytic nanoparticles. *J Endod*. 2018;44(5):806-812.
79. Shrivastava R, Kushwaha P, Bhutia YC, Flora S. Oxidative stress following exposure to silver and gold nanoparticles in mice. *Toxicol Ind Health*. 2016;32(8):1391-1404.
80. van der Zande M, Vandebriel RJ, Van Doren E, et al. Distribution, elimination, and toxicity of silver nanoparticles and silver ions in rats after 28-day oral exposure. *ACS Nano*. 2012;6(8):7427-7442.
81. Wang J, Zhou G, Chen C, et al. Acute toxicity and biodistribution of different sized titanium dioxide particles in mice after oral administration. *Toxicol Lett*. 2007;168(2):176-185.
82. Chen Z, Meng H, Xing G, et al. Acute toxicological effects of copper nanoparticles *in vivo*. *Toxicol Lett*. 2006;163(2):109-120.

83. Trouiller B, Reliene R, Westbrook A, Solaimani P, Schiestl RH. Titanium dioxide nanoparticles induce DNA damage and genetic instability *in vivo* in mice. *Cancer Res.* 2009;69(22):8784-8789.